National Library of Canada
Acquisitions and Bibliographic Services Branch
395 Wellington Street
Ottawa, Ontario
K1A 0N4

Bibliothèque nationale du Canada
Direction des acquisitions et des services bibliographiques
395, rue Wellington
Ottawa (Ontario)
K1A 0N4

Your file Votre référence

Our file Notre référence

NOTICE

The quality of this microform is heavily dependent upon the quality of the original thesis submitted for microfilming. Every effort has been made to ensure the highest quality of reproduction possible.

If pages are missing, contact the university which granted the degree.

Some pages may have indistinct print especially if the original pages were typed with a poor typewriter ribbon or if the university sent us an inferior photocopy.

Reproduction in full or in part of this microform is governed by the Canadian Copyright Act, R.S.C. 1970, c. C-30, and subsequent amendments.

AVIS

La qualité de cette microforme dépend grandement de la qualité de la thèse soumise au microfilmage. Nous avons tout fait pour assurer une qualité supérieure de reproduction.

S'il manque des pages, veuillez communiquer avec l'université qui a conféré le grade.

La qualité d'impression de certaines pages peut laisser à désirer, surtout si les pages originales ont été dactylographiées à l'aide d'un ruban usé ou si l'université nous a fait parvenir une photocopie de qualité inférieure.

La reproduction, même partielle, de cette microforme est soumise à la Loi canadienne sur le droit d'auteur, SRC 1970, c. C-30, et ses amendements subséquents.

Canada

UNIVERSITY OF ALBERTA

SULFIDATION OF BANDED IRON FORMATION, AND GOLD DEPOSITION AT GEORGE LAKE, N.W.T.

by

BARBARA A. HENDERSON

A thesis submitted to the Faculty of Graduate Studies and Research in partial fulfilment of the requirements for the degree of Master of Science.

DEPARTMENT OF GEOLOGY

Edmonton, Alberta
Fall 1993

National Library
of Canada

Acquisitions and
Bibliographic Services Branch

395 Wellington Street
Ottawa, Ontario
K1A 0N4

Bibliothèque nationale
du Canada

Direction des acquisitions et
des services bibliographiques

395, rue Wellington
Ottawa (Ontario)
K1A 0N4

Your file Votre référence

Our file Notre référence

The author has granted an irrevocable non-exclusive licence allowing the National Library of Canada to reproduce, loan, distribute or sell copies of his/her thesis by any means and in any form or format, making this thesis available to interested persons.

L'auteur a accordé une licence irrévocable et non exclusive permettant à la Bibliothèque nationale du Canada de reproduire, prêter, distribuer ou vendre des copies de sa thèse de quelque manière et sous quelque forme que ce soit pour mettre des exemplaires de cette thèse à la disposition des personnes intéressées.

The author retains ownership of the copyright in his/her thesis. Neither the thesis nor substantial extracts from it may be printed or otherwise reproduced without his/her permission.

L'auteur conserve la propriété du droit d'auteur qui protège sa thèse. Ni la thèse ni des extraits substantiels de celle-ci ne doivent être imprimés ou autrement reproduits sans son autorisation.

ISBN 0-315-88418-5

Canada

UNIVERSITY OF ALBERTA

RELEASE FORM

Name of Author: BARBARA A. HENDERSON

Title of Thesis: SULFIDATION OF BANDED IRON FORMATION, AND GOLD DEPOSITION AT GEORGE LAKE, N.W.T.

Degree: MASTER OF SCIENCE

Year This Degree Granted: 1993

Permission is hereby granted to the University of Alberta Library to reproduce single copies of this thesis and to lend or sell such copies for private, scholarly or scientific research purposes only.

The author reserves all other publication and other rights in association with the copyright in the thesis, and except as hereinbefore provided neither the thesis nor any substantial portion thereof may be printed or otherwise reproduced in any material form whatever without the author's prior written permission.

#210, 8604 - 103 St.
Edmonton, AB
Canada
T6E 4B6

Dated June 11/93

UNIVERSITY OF ALBERTA

FACULTY OF GRADUATE STUDIES AND RESEARCH

The undersigned certify that they have read, and recommend to the Faculty of Graduate Studies and Research for acceptance, a thesis entitled Sulfidation of Banded Iron Formation, and Gold Deposition at George Lake, N.W.T. submitted by Barbara A. Henderson in partial fulfilment of the requirements for the degree of Master of Science.

Dr. B.E. Nesbitt

Dr. T. Chacko

Dr. R. Creaser

Dr. J. Whiting

Dated MAY 27 1993

ABSTRACT

The George Lake property contains five banded iron formation-hosted gold deposits. On the property, Archean turbidite sequences host Silicate- and Oxide Iron Formation (OIF). Gold-bearing zones are restricted to the iron formation, and primarily occur in the OIF as haloes surrounding late quartz veins.

Unmineralized OIF (nil to trace sulfides) grades into mineralized OIF (1 to 50 percent sulfides) as a quartz vein is approached. Unmineralized OIF consists of recrystallized chert, grunerite, stilpnomelane, magnetite, hornblende and chlorite. The transition to mineralized OIF is marked by an increase in the abundances of hornblende and chlorite, the replacement of magnetite by pyrrhotite, and the appearance of arsenopyrite and gold. The spatial association of mineralized OIF with quartz veins, and the observed replacement of magnetite by pyrrhotite, suggests that gold deposition at George Lake is epigenetic, and a result of sulfidation.

Microprobe analyses of gruneries from unmineralized and mineralized OIF show that the stoichiometric ratios of Fe to Mg do not vary with mineralization. The X_{Fe} (Fe/(Fe+Mg)) of gruneries from unmineralized OIF ranges from 0.72 to 0.86 and averages 0.80 +/- 1σ. For gruneries from mineralized OIF, the X_{Fe} range is 0.74 to 0.84, and average is 0.81 +/- 1σ. Due to the lack of a shift in X_{Fe} values of gruneries with increased sulfide content, it is interpreted that the primary source of iron for the sulfidation process at George Lake was magnetite.

The deposition of gold at George Lake involved the introduction of fluids to the iron formation via structural conduits. These fluids carried gold as bisulfide complexes and had an f_{O2} in approximate equilibrium with the iron formation. As these fluids infiltrated the OIF, sulfur from the fluids reacted with magnetite to form pyrrhotite, thereby destabilizing the bisulfide complex and causing the deposition of gold. This model accounts for the close proximity of gold-bearing zones to quartz veins, the observed replacement of magnetite by

pyrrhotite, the close association of gold values with sulfide content, and the constancy of the grunerite X_{Fe} values in unmineralized and mineralized OIF.

ACKNOWLEDGEMENTS

Numerous individuals and organizations are deserving of thanks for their support, in various forms, in the completion of this project.

I would like to thank Dr. Bruce Nesbitt for supervising this project. From his original suggestion for this study, to the final days of its completion, Bruce has always made time to help me out. This project would not have been possible without the permission and financial support of the co-owners of the George Lake property; Homestake Mineral Development Co. and Kerr-McGee Corp. Discussions with, and input from Terry Chandler (HMDC) and Harold Holmberg (KM) were enlightening and their suggestions, as well as those of Ken Rye (HMDC) were quite helpful in the progression of this study. In addition, I would like to thank Reg Olson of R.A. Olson Consulting Ltd. for his discussions on the background and early stages of exploration at George Lake.

Many thanks to Paul Wagner and Dr. Tom Chacko, and my fellow graduate students for their help, understanding and advice, and for helping to make my time at the University of Alberta a lot of fun. My family, Janice, Michael and Jan, Brian, and David, have given me much needed support and encouragement throughout my education. Lastly I would like to thank Rob for his help and support throughout this project, especially in its final stages, and for encouraging me to realize my potential. Cheers everyone.

TABLE OF CONTENTS

	page
ABSTRACT	i
ACKNOWLEDGEMENTS	iii
CHAPTER 1: INTRODUCTION	1
Models for the Formation of Banded Iron Formation-Hosted Gold Deposits	1
Previous Work on Banded Iron Formation-Hosted Gold Deposits	4
Scope of This Study	5
Methods	6
CHAPTER 2: GEOLOGY	7
Regional Geology	7
Geology of the George Lake Area	11
CHAPTER 3: PETROGRAPHY	16
Microscopic Observations	16
Petrological Relationships	20
Unmineralized and Mineralized OIF	23
Paragenetic Sequence	24
Genetic Model for Gold Deposition at George Lake	27
CHAPTER 4: PROCESSES OF GOLD DEPOSITION	28
Sulfidation	28
Mineral Chemistry	29

page

CHAPTER 5: DISCUSSION AND CONCLUSIONS 37

Mineral Equilibria in the FeO-FeS System 39

Interpretation of the Sulfidation Process based on Mineral Stabilities and Reaction Equilibria 40

Comparison of George Lake to the Lupin Deposit 45

CHAPTER 6: CONCLUSIONS AND RECOMMENDATIONS 48

Conclusions 48

Recommendations 50

REFERENCES 52

APPENDIX 1: MINERAL INVENTORY 56

APPENDIX 2: MICROPROBE ANALYSES 61

LIST OF TABLES

page

TABLE 1. Representative microprobe analyses of grunerites from unmineralized OIF..... 31

TABLE 2. Representative microprobe analyses of grunerites from mineralized OIF..... 32

LIST OF FIGURES

page

Fig. 1. Key features of Epigenetic and Modified Syngenetic BIF-hosted gold deposits..... 3

Fig. 2. The Slave Structural Province..... 8

Fig. 3. Stratigraphic relationships between the Hackett River, Beechy Lake, and Back Groups in the Hackett River Area, N.W.T..... 10

Fig. 4. Simplified geology of the George Lake Property..... 12

Fig. 5. Typical stratigraphic setting of iron formation at George Lake... 15

Fig. 6. Geometry of the George Lake belt..... 15

Fig. 7. Stoichiometric values of Fe versus Mg..... 33

Fig. 8. Histogram of X_{Fe} values of grunerites from unmineralized OIF.. 35

Fig. 9. Histogram of X_{Fe} values of grunerites from mineralized OIF..... 36

Fig. 10. Log fO_2 vs. log fS_2 diagram for the FeO-FeS system at 600 K and 2kbars, with contours of X_{Fe} of grunerite..... 41

Fig. 11. Enlargement of Fig. 10 for region of interest at George Lake.. 41

Fig. 12. Possible relationship between Lupin and George Lake rock geochemistry pathways..... 46

LIST OF PLATES

page

Plate 1. Recrystallized chert and vein quartz..... 17

Plate 2. Feather-shaped grunerite rimmed with hornblende..... 17

Plate 3. Biotite grain grown around pyrrhotite..... 19

Plate 4. Blocky patches of graphite laminations..... 19

Plate 5. Magnetite grains rimmed with pyrrhotite..... 21

Plate 6. Visible gold in fracture with pyrrhotite in arsenopyrite..... 21

Plate 7. Unmineralized OIF..... 25

Plate 8. Transition from unmineralized to mineralized OIF..... 25

Plate 9. Mineralized OIF..... 26

CHAPTER 1
INTRODUCTION

The George Lake property (George Lake) contains numerous banded iron formation (BIF)-hosted gold deposits and occurrences. The property, located 515 kilometres northeast of Yellowknife and 175 kilometres east of the Lupin gold mine, is currently held by the George Lake Joint Venture, consisting of Homestake Mineral Development Company and Kerr-McGee Corporation.

Auriferous iron formation in the George Lake area was discovered by Trigg Woollett Olson Consulting Limited in 1982. Reconnaissance exploration, including geological mapping, sampling and geophysics followed this discovery, and from 1985 to 1991, extensive diamond drilling programs were undertaken. To date, over 105 000 metres of core in 572 holes have been recovered from the property. It is currently estimated that George Lake hosts reserves of 3.4 million tons, grading 0.35 ounces of gold per ton.

Both Silicate- and Oxide Iron Formation occur at George Lake, and are interlayered with meta-turbidites of the Archean Beechy Lake Group (Chandler and Holmberg 1992). Although anomalous gold concentrations occur in both types of iron formation, the largest and most economically significant gold deposits are located in the Oxide Iron Formation, generally within 10 to 12 metres of the stratigraphic base of this unit (Chandler and Holmberg 1992). Gold-bearing zones are associated with sulfide concentrations and occur as halos surrounding one or more quartz veins. The principal objective of this thesis is to determine the nature of the processes that led to the deposition of gold in the Oxide Iron Formation at George Lake.

Models for the Formation of Banded Iron Formation-Hosted Gold Deposits

There are currently three genetic models for banded iron formation-hosted gold deposits; 1) a syngenetic model, in which gold is a primary constituent of the iron formation, 2) a modified syngenetic model which invokes a syngenetic origin for gold in the iron formation, with later remobilization and

concentration during metamorphism, and 3) an epigenetic model in which gold is introduced to the iron formation later via hydrothermal fluids (Lhotka 1988, Groves et al. 1987).

The stratabound nature of most of the banded iron formation-hosted gold deposits is often cited as evidence supporting the syngenetic and modified syngenetic models (Fripp 1976). However, most deposits, including George Lake, also show a strong structural control, with gold-bearing zones centred around faults, fractures and/or quartz veins (Phillips et al. 1984). The stratabound nature of the deposits can be accounted for by all three genetic models. However, the structural affiliation of gold-bearing zones can only be explained by the modified syngenetic and epigenetic models. These models are therefore most commonly invoked, although numerous controversies persist regarding which model best accounts for the features of some banded iron formation-hosted gold deposits.

Criteria to distinguish epigenetic- from syngenetic-type deposits have been established by several authors (Kerswill 1992, Groves et al. 1987, Phillips et al. 1984, and others). However, epigenetic and modified syngenetic processes would produced deposits similar in character (Fig. 1), and few criteria exist to discriminate between these two models. Two examples of such criteria, that may be of use in solving this dilemma, are summarized below.

According to both models, gold concentrations are centred around late structures, including quartz veins. The modified syngenetic model proposes that the source of the gold is the banded iron formation itself. Unless the iron formation was completely depleted of its primary gold, anomalously high gold concentrations should be found away from the late structures in a modified syngenetic-type deposit (Groves et al. 1987). Conversely, the iron formation outside of main gold-bearing zones should be barren of gold in an epigenetic-type deposit.

There is a close association between gold and iron-sulfide concentrations in most banded iron formation-hosted gold deposits, indicating that the two are synchronous (Groves et al. 1987). Therefore, if the genesis of the iron-sulfides

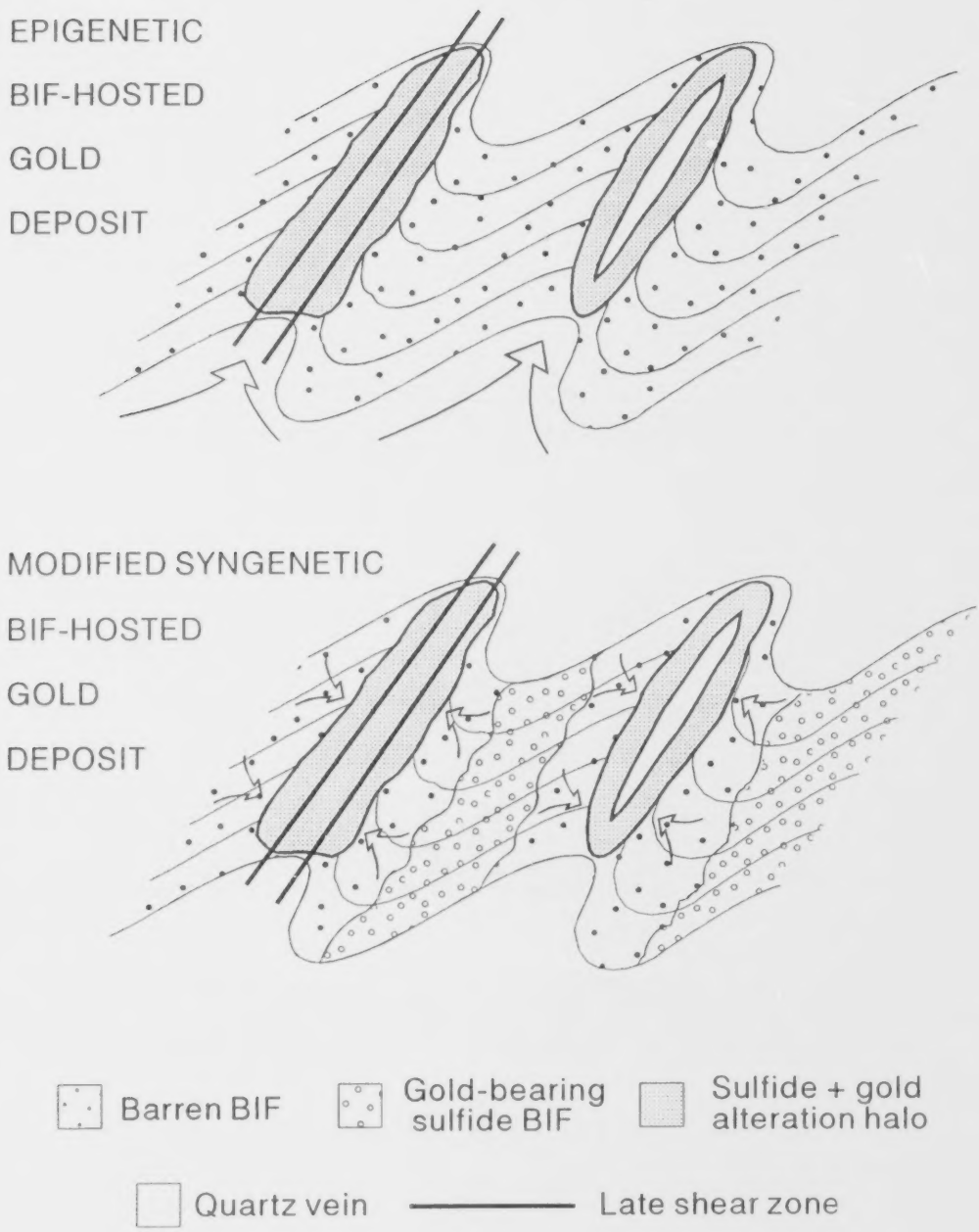

Fig. 1. Key features of Epigenetic and Modified Syngenetic BIF-hosted gold deposits. In the epigenetic model, gold and sulfides are introduced to barren BIF via hydrothermal fluids, while in the modified syngenetic model, gold and sulfides are remobilized from gold-bearing sulfide BIF. In both cases, the gold and sulfides are deposited in haloes around late structures. (modified from Kerswill 1992)

can be determined, so too can the genesis of the gold. A banded iron formation-hosted gold deposit in which the iron sulfides associated with the gold are primary, would indicate a modified syngenetic deposit, whereas one in which the sulfides are clearly secondary, would indicate epigenetic processes. These two criteria will be employed in this thesis to determine which model is best applied to the gold deposits at George Lake.

Previous Work on Banded Iron Formation-Hosted Gold Deposits

Banded iron formation-hosted gold deposits occur worldwide, and have been the focus of numerous studies. Recent work has focused on the processes responsible for the deposition of gold in these banded iron formations, and several well known Archean examples are discussed below.

Banded iron formation is interlayered with mafic and felsic volcanic tuffs in the Vubachikwe mine in Zimbabwe. Both carbonate- and sulfide iron formation host stratiform and lenticular, gold-rich ore bodies (Fripp 1976). The stratiform nature of the deposit is cited by Fripp (1976) as evidence that the gold in this deposit is syngenetic. Phillips et al. (1984) contest this conclusion and suggest that this deposit is in fact epigenetic. They refer to the presence of gold- and arsenopyrite-bearing halos around quartz veins as evidence for their conclusion.

Groves et al. (1987) and Phillips et al. (1984) are strong proponents of the epigenetic model for the Water Tank Hill deposit in Western Australia. They suggest that hydrothermal fluids, also responsible for vein- and shear zone-related gold deposits in nearby volcanics, infiltrated oxide iron formation. Upon contact with the iron formation, a sulfidation reaction occurred whereby gold and iron-sulfides were deposited from the fluids. Evidence for this model includes the replacement of magnetite by pyrrhotite adjacent to quartz + pyrrhotite veins, the carbonatization of wall rock adjacent to the veins, and low background values for gold in the banded iron formation (Groves et al. 1987).

The Homestake mine in South Dakota is the largest known iron formation-hosted gold deposit (Caddey et al. 1991). The deposit is hosted in

quartz-veined, sulfide-rich carbonate iron formation. Tabular to pipe-shaped ore bodies consist of quartz, siderite, chlorite, pyrrhotite, arsenopyrite and pyrite (Caddey et al. 1991). Rye and Rye (1974) used sulfur and oxygen isotope ratios to support a modified syngenetic process of gold deposition at the Homestake mine. However, Caddey et al. (1991) have interpreted this deposit as epigenetic, based primarily on the structural control of the ore bodies.

The Lupin mine is a major banded iron formation-hosted gold deposit in the Slave Structural Province, N.W.T. In the Lupin area, banded iron formation beds occur as tight to isoclinal north- to northwesterly-trending folds. The orebody itself consists of the West, Main and East zones, which constitute the limbs of a Z-fold defined by the iron formation, and contains sulfide-, silicate-, and oxide iron formation (Lhotka and Nesbitt 1989). Lhotka and Nesbitt (1989) report that gold-bearing zones are intimately associated with quartz veins and attendant sulfide concentrations, and that unmineralized (nil to trace sulfides and gold) zones occur farther away from the veins. These authors propose that these features, as well as the relative depletion of iron in iron-silicates from mineralized zones, indicates that the deposit was formed by epigenetic processes. Kerswill (1984, 1986) and Padgham (1992) however, disagree. These authors state that the Lupin orebody is stratiform, and that unmineralized portions of the orebody are rare. A modified syngenetic model is favoured by Kerswill (1984, 1986, 1992), in which gold was deposited simultaneously with sulfide iron formation, and was later locally remobilized along with arsenic and silica during the formation of quartz veins.

Scope of this Study

The apparent association of gold-bearing zones with quartz veins and sulfide concentrations in the oxide iron formation at George Lake has been noted by geologists working on the property since its discovery. However, this association has not been confirmed in detail. This study is composed of two basic parts. First, detailed thin section analysis was used to determine whether the gold - quartz vein - sulfide association observed macroscopically could be

upheld petrographically. The criteria described earlier was then applied to determine which genetic model best applies to the deposits at George Lake. Secondly, iron-silicates were analyzed to determine whether a relationship exists between their mineral chemistry and the degree of mineralization. This investigation followed the example of Lhotka (1988) who used evidence of such a relationship to help determine the process of gold deposition at the Lupin mine.

The results of these studies provide a comprehensive understanding of the processes responsible for the deposition of gold at George Lake, which in turn may help guide future exploration in the area.

Methods

Fieldwork for this study took place during the summer of 1990 and consisted primarily of logging core for Homestake Mineral Development Co., the operators of the George Lake project at that time. Core logging provided the opportunity to study and understand the rock units of George Lake, especially the relationship between mineralized and unmineralized iron formation. During this period, macroscopic observations of mineralized and unmineralized iron formation were recorded and 261 samples were taken.

Petrographic analysis under normal and reflective light was completed on 127 polished thin sections of unmineralized, transitional and mineralized iron formation.

Numerous mineral grains from 30 polished thin sections were analyzed on an ARL-SEMQ electron microprobe for either quantitative analysis or for verification of mineral identification. Wavelength Dispersive Analysis was conducted primarily on grunerite and hornblende grains using a natural Kakanui kaersutite standard. Depending on the size of the grain being probed, the beam ranged in diameter from 1 to 10 microns. The Bence Albee method of data reduction was used, with final element weight percentages based on 23 oxygens per formula unit.

CHAPTER 2
GEOLOGY

Regional Geology

The Slave Structural Province (Fig. 2), an Archean granite-greenstone terrane in the Northwest Territories, has been the subject of abundant lithostratigraphic, structural and metamorphic studies and has been found to host numerous precious and base metal deposits (McGlynn and Henderson 1972, McGlynn 1977, Hoffman 1989, Padgham and Fyson 1992, and others). Archean rocks of the Slave province include: 1) pre-2.8 Ga basement rocks consisting of migmatites, gneisses and highly deformed granitoids, which are thought to underlie much of the western part of the Slave (Card and King 1992), 2) mature clastic sediments (the Old Shelf Assemblage of Padgham (1992)), including quartz-arenite, quartz pebble conglomerates, felsic volcanics and quartz-magnetite iron formation, 3) Yellowknife Supergroup rocks which include mafic and felsic volcanics, turbidites and chemical sediments of the Volcanic-Turbidite Series (VTS) (Padgham 1992) and syn- and post-VTS granitoids and migmatites, and 4) post-VTS conglomerates and sandstones (Padgham 1992, Card and King 1992).

Volcanic-Turbidite Series rocks (2.7 to 2.65 Ga), the most widespread and abundant supracrustal units in the Slave, are dominated by large areas of turbidite that are flanked by narrow volcanic belts and include distinct volcanic complexes (Padgham and Fyson 1992, Padgham 1992). Interlayering of volcanic units with greywacke and mudstone indicates that volcanism was contemporaneous with high-energy sedimentation throughout the Slave (Padgham and Fyson 1992). Two "types" of volcanics have been identified in the Slave. Hackett River-type volcanics are felsic to intermediate in composition and of calc-alkaline affinity, whereas Yellowknife-type volcanics are intermediate to mafic in composition and display tholeiitic differentiation trends (Padgham 1992).

The Hackett River area is located in the northeastern Slave Province

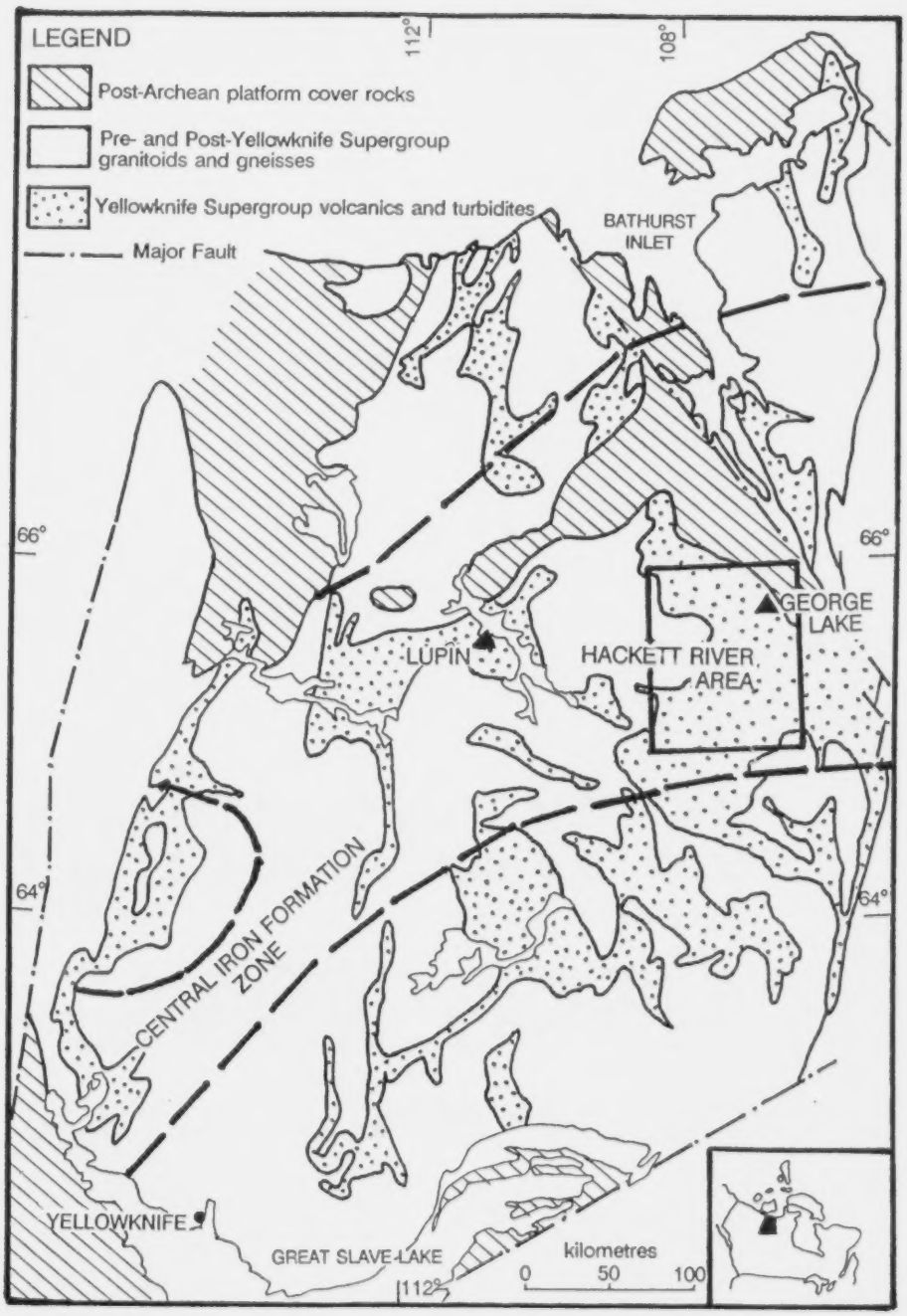

Fig. 2. The Slave Structural Province.
(modified from Padgham 1992, Padgham and Fyson 1992, and Frith 1987)

(Fig. 2). The area was mapped selectively by Tremblay (1971) and systematically by Frith and Percival (1978) and Frith (1987), and was found to contain rocks of the Yellowknife Supergroup (both VTS and later plutonics) and small exposures
of the overlying Proterozoic Goldburn Group. Frith and Percival (1978) and Frith (1987) divided Yellowknife Supergroup rocks into the Hackett River, Beechy Lake and Back Groups, and determined the following stratigraphic relationships (Fig. 3a). The Hackett River Group contains a basal volcanogenic metasedimentary unit with overlying subaqueous and subaerial Hackett River-type volcanics and pyroclastics. They are conformably overlain by the Beechy Lake Group, which includes homogenous, well bedded greywackes and mudstones and minor carbonaceous mudstone, pyroclastics and silicate and oxide iron formation. The Back Group, defined by Frith and Percival (1978), unconformably overlies the Beechy Lake Group and consists of basalt and andesite flows, dacite volcanic domes and felsic pyroclastics.

During the Archean, these units underwent three periods of deformation including; large scale folding and downwarping of volcanic margins (D1), later formation of uplifted regions and concomitant foliation development (D2) when regional thermal metamorphism was at its peak, and lastly formation of a subvertical foliation (D3) (Frith 1987). In the area, metamorphism ranges from greenschist to upper amphibolite facies (Frith 1987).

The initial stratigraphic relationships were later revised by Jefferson et al. (1989) and Lambert et al. (1990), who suggested that the Back Group and upper parts of the Hackett River Group were coeval and that these volcanics were both interfingered with, and overlain by the Beechy Lake Group (Fig. 3b). This interpretation was based on detailed stratigraphic studies of sedimentary (Jefferson et al. 1989) and volcanic (Lambert et al. 1990) units in both the Hackett River area and the Back River Volcanic Complex 18 km to the south. A model for the evolution of these groups includes volcanism punctuated by erosion and periods of fluvial fan deposition, as indicated by the intimate interbedding of Hackett River and Back River Group volcanics with Beechy Lake

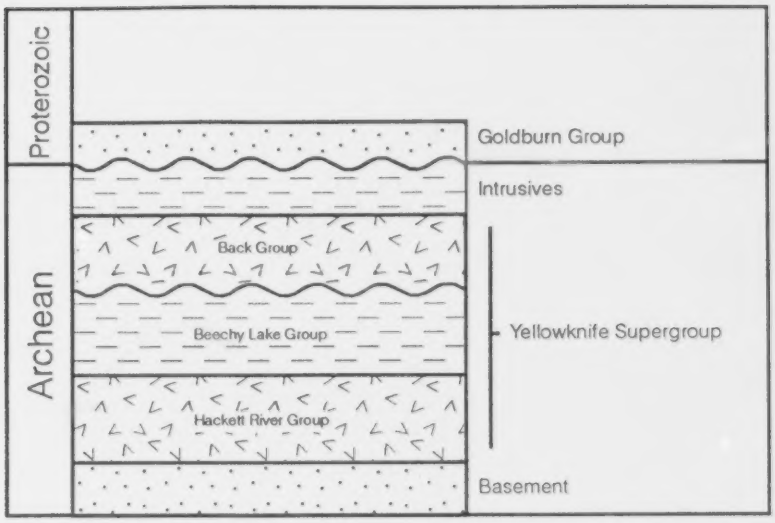

a

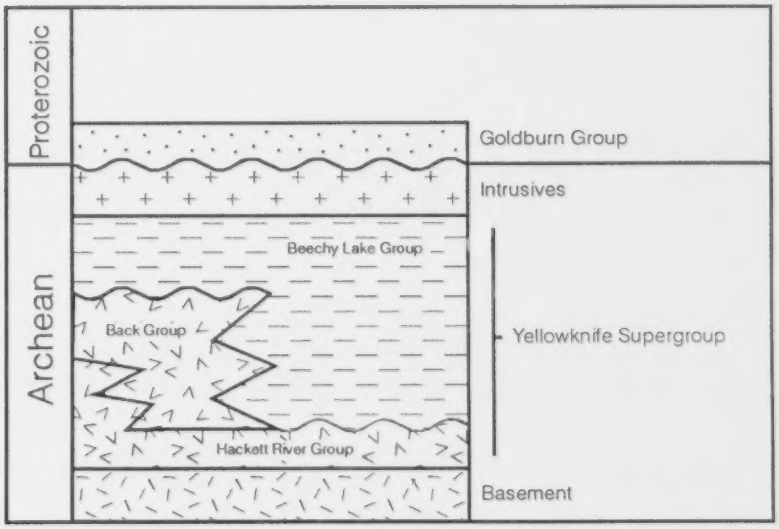

b

Fig. 3. Stratigraphic relationships between the Hackett River, Beechy Lake, and Back Groups in the Hackett River Area, N.W.T.
a) Initial interpretation (modified from Frith and Percival 1978)
b) Current interpretation (modified from Lambert et al. 1990 and Jefferson et al. 1989)

Group sediments (Lambert et al. 1990).

Lambert et al. (1990), Jefferson et al. (1989) and Jefferson et al. (1990) describe three chemical sedimentary sequences which punctuate volcanic and sedimentary units of the Back River Volcanic Complex. The earliest sequence (Sequence A) is dominated by sulfide-bearing volcaniclastics, slate and iron formation and is hosted in volcanics. Sequence B consists primarily of cherty magnetite, sulfide and siderite iron formation, with minor carbonates, volcaniclastics, slates and turbidites. The latest sequence (Sequence C) is hosted by turbidites of the Beechy Lake Group and includes argillitic to cherty magnetite iron formation with a pronounced magnetic signature, minor silicate and sulfide iron formation, and graphitic slates.

Generally, iron formation is only locally abundant in VTS rocks of the Slave province (Padgham 1992). Turbidite-hosted iron formation (Sequence C in the Back River Volcanic Complex) is restricted mainly to the Central Iron Formation Zone (Fig. 2). These iron formations host most of the stratiform and stratabound gold prospects in the northeastern Slave province (Jefferson et al. 1990).

The George Lake property (George Lake), located in the northeastern corner of the Hackett River area (Fig. 2), contains oxide- and silicate iron formation hosted in Beechy Lake Group turbidites. These iron formations are similar both in mineralogy and stratigraphic setting to Sequence C iron formations of the Back River Volcanic Complex (Jefferson et al. 1992).

Geology of the George Lake Area

A simplified geological map of George Lake is shown in Fig. 4. The area consists of Beechy Lake Group greywacke and mudstone, iron formations, a sheared quartz-feldspar porphyry, Archean felsic to intermediate dykes, and mafic Helikian dykes. These units are unconformably overlain to the northeast by the Proterozoic Goldburn Group.

Three belts of iron formation are contained within the greywacke and mudstone. These belts (the George Lake belt, the Fold Nose belt and the

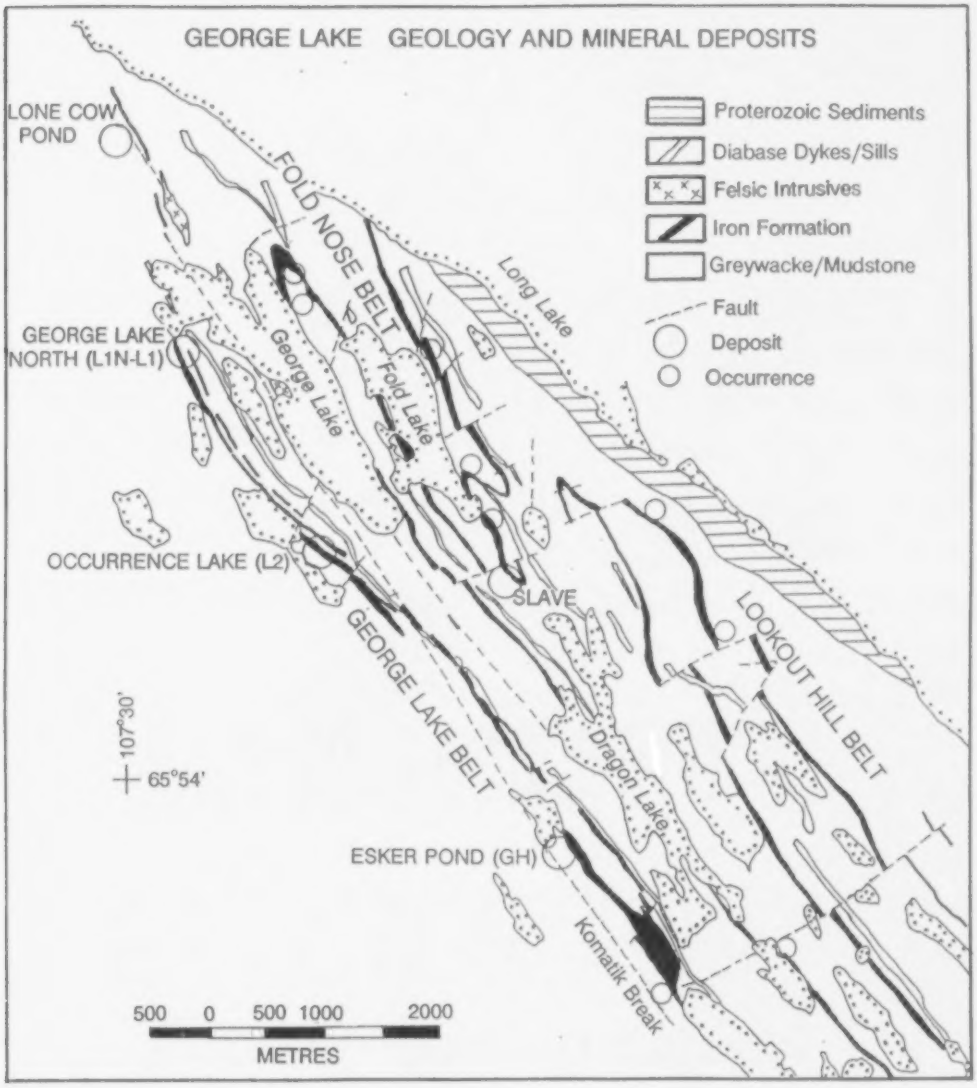

Fig. 4. Simplified geology of the George Lake property.
(modified from Chandler and Holmberg 1990, and Jefferson et al. 1992)

Lookout Hill belt) are spatially distinct, although they may represent one continuous belt of iron formation that has been broken apart by folding and faulting (Chandler and Holmberg 1990). Iron formation at George Lake is of two types; oxide iron formation (chert, magnetite and grunerite dominated) and silicate iron formation (chert, grunerite and chlorite dominated). A typical stratigraphic section showing the setting of these iron formations is shown in Fig. 5, and is consistent between all three belts (Chandler and Holmberg 1990). Oxide- and silicate iron formation commonly occur as separate and distinct units, although they locally grade into each other as a function of magnetite depletion or enrichment.

The deformation history of rocks at George lake is complex. Two periods of faulting have been recognized; an early northwest-trending, bedding-sub-parallel set of brittle faults to ductile shear zones, on which a sense of movement is difficult to determine, and a later north to northeast-trending set of brittle faults that are steeply dipping and show both sinistral and dextral offsetting of stratigraphy (Chandler and Holmberg 1990). Major folds at George lake are tight to isoclinal, with steep west-dipping axial planes and sub-horizontal fold axes. Fold axes plunge to both the northwest and southeast, indicating that the present fold geometry is likely the result of refolding of an earlier event. Lastly, late deformation produced wide open folding along north to northeast fold axes (Chandler and Holmberg 1990). Metamorphic grade in the area is low to middle greenschist facies, as indicated by the presence of biotite and ubiquitous chlorite (Chandler and Holmberg 1990).

van Breeman et al. (1992) present the results of U-Pb dating of zircons from rhyolite bodies that intrude the turbidites, which host the iron formation, and detrital zircons from a granulestone interbed in the turbidites. The two ages obtained are in close agreement, enabling the age of the iron formations to be precisely determined at 2683 +/- 1.5 Ma (van Breeman et al. 1992).

Five major gold deposits and numerous occurrences have been discovered in the iron formation at George Lake (Fig. 4). These occurrences occur exclusively within the iron formation and the largest deposits are

restricted to the oxide iron formation. Although all three belts contain occurrences, the George Lake belt appears to be the most promising economically as it contains three of the five large deposits; George Lake North (L1N), Occurrence Lake (L2) and Esker Pond (GH) (Chandler and Holmberg 1990).

The geometry of the George Lake belt is shown in Fig. 6. This belt consists of a slightly overturned, west-dipping, tight synclinal fold. Gold-bearing zones at L1N and L2 (the area covered in this study) are generally restricted to within 10-12 metres of the western edge of the oxide iron formation, at its stratigraphic base. To date, negligible gold or sulfide mineralization has been noted in the oxide iron formation on the eastern limb of this fold (Chandler and Holmberg 1990). The oxide iron formation along the western limb appears to be tabular, and the stratigraphic section shown in Fig. 5 is consistent along the strike of the belt. However, close examination of the iron formation shows it to be complexly folded internally, producing marked variations in its thickness along the strike of the belt (Chandler and Holmberg 1990).

Gold-bearing zones within this oxide iron formation tend to occur as 1-10 metre wide shoots and are accompanied by sulfide concentrations associated with quartz veins. Visible gold is common both at surface and in drill core, and is often intimately associated with sulfides such as pyrrhotite, arsenopyrite or pyrite, or within the chloritic alteration halo surrounding a quartz vein. Sulfide content of the gold-bearing zones averages 5%, but locally reaches up to 50% (Chandler and Holmberg 1990).

Quartz veins, which also commonly contain carbonates, occur in three sets and are more abundant in the iron formations than in the surrounding sediments. Although most gold-bearing zones occur in a 1-5 metre halo surrounding quartz veining, not all veins have attendant sulfide or gold mineralization associated with them (Chandler and Holmberg 1990).

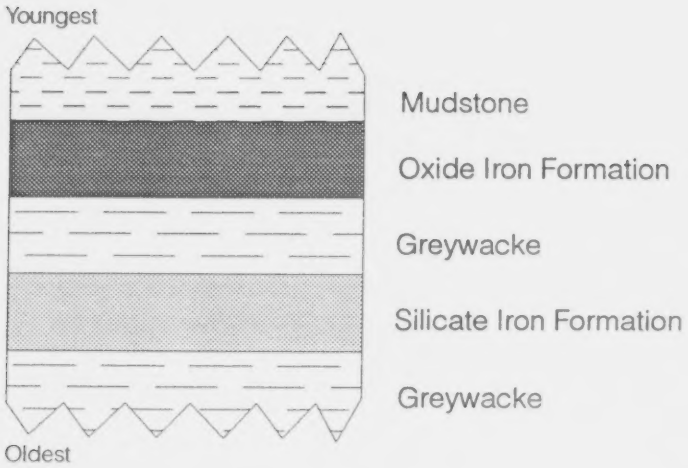

Fig. 5. Typical stratigraphic setting of iron formation at George Lake. (modified from Chandler and Holmberg 1990)

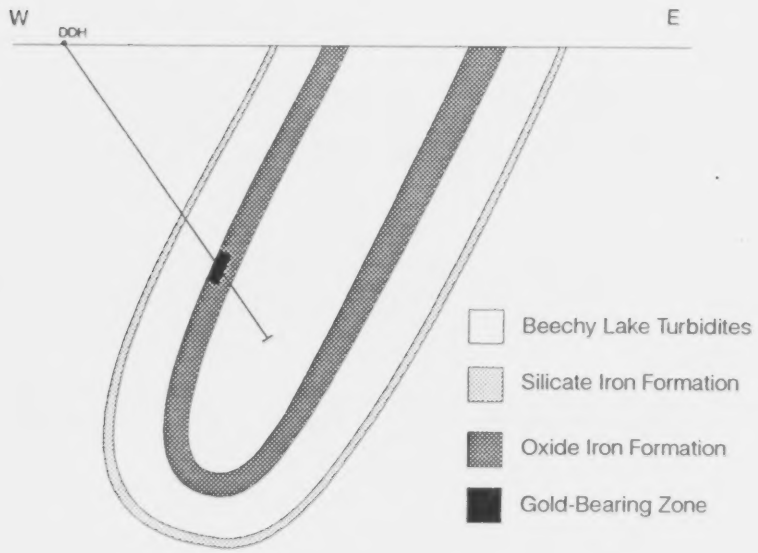

Fig. 6. Geometry of the George Lake belt

CHAPTER 3
PETROGRAPHY

A petrographic study was undertaken to determine the mineralogy, textures and petrogenetic sequence of unmineralized and mineralized oxide iron formation. The samples used in this study were obtained from L1N and L2 of the George Lake belt (Fig. 4) as this area was the focus of abundant diamond drilling, allowing for easy access to a wide range of sample types and locations. Oxide iron formation (OIF) was targeted specifically since on the western limb of the George Lake belt, the OIF is locally gold-bearing. This provided the opportunity to study both unmineralized (with nil to trace sulfides) and mineralized (with 1-50% sulfides) examples of OIF, as well as the petrographic transition between the two.

Microscopic Observations

Microscopic observations were made on 127 polished thin sections of unmineralized and mineralized OIF drill core samples obtained from L1N and L2. The mineralogy (see Appendix 1) and textures from each sample were recorded and a paragenetic sequence based on these observations was developed. The mineralogy of the samples is surprisingly consistent, with the exception of magnetite and sulfides, for both unmineralized and mineralized OIF. A review of the mineralogic characteristics is presented below.

Quartz, as recrystallized chert or vein quartz (Plate 1), is present in virtually all of the samples. Recrystallized chert occurs as 0.05-0.2 mm wide grains with straight boundaries, triple junctions and flat-field extinction, and often contains very fine-grained stilpnomelane needles, grunerite rosettes, ferroan calcite, or magnetite. Vein quartz grains are 0.3-5 mm wide, have irregular, often sutured boundaries and undulose extinction. This type of quartz is not restricted to veins, but is sometimes found penetrating the wallrock adjacent to veins. Carbonate minerals were difficult to identify with thin sections alone, and required microprobe analysis for specific identification. Three varieties of

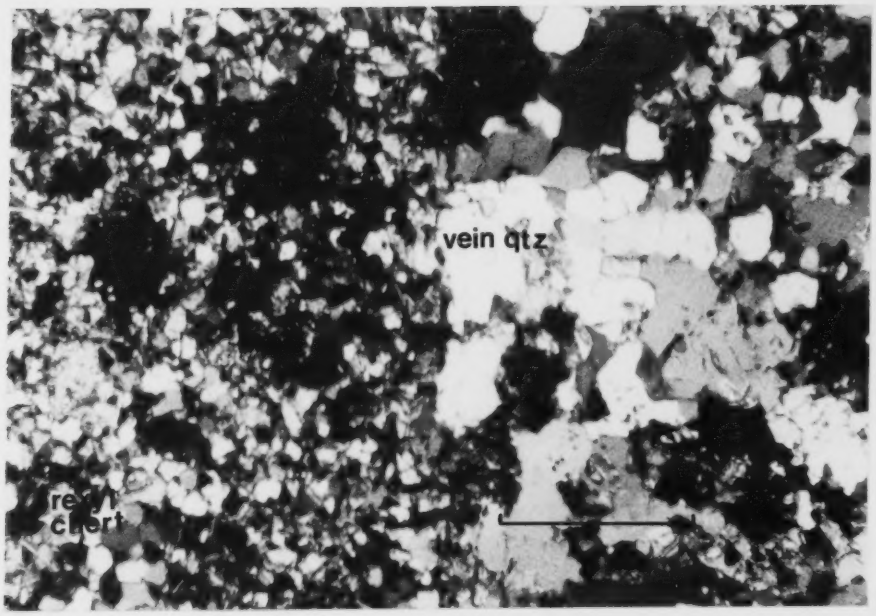

Plate 1. Recrystallized chert and vein quartz
Taken in cross-polarized light. Scale bar = 1mm

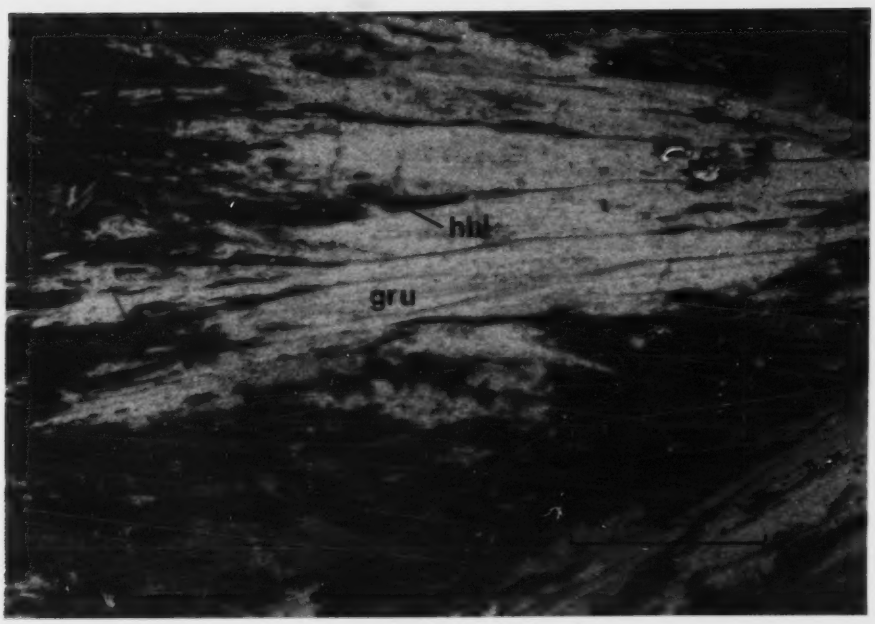

Plate 2. Feather-shaped grunerite rimmed with hornblende
Taken in plane-polarized light. Scale bar = 1mm

carbonate exist in the samples: 1) ferroan calcite ($CaCO_3$ with 1-2 weight % Fe), 2) ankerite, and 3) siderite, with ferroan calcite being the most common. Carbonates occur as groundmass constituents, or in veins with or without quartz. Groundmass carbonates are 0.3-0.7 mm wide, anhedral and contain included quartz, magnetite, graphite, or stilpnomelane. Glide twins in these grains are uncommon. Most groundmass carbonate is ferroan calcite, and locally these grains rim, or form the core to grunerite rosettes. Vein carbonate grains are 0.5-5 mm wide, anhedral to subhedral and tabular in form, and are inclusion-free. Glide twins at 60° and 120° are common. Vein carbonate is primarily ankerite, although some siderite and ferroan calcite is also present. As with the vein quartz, vein carbonate is sometimes noted within the wallrock adjacent to the vein.

Grunerite occurs as 0.3-4 mm long, radiating tabular or feather-shaped grains, and as circular rosettes. This mineral is often rimmed by hornblende, and frequently contains zircon inclusions (Plate 2). Hornblende, although present in L1N rocks, is most commonly noted in rocks from L2, where it is found on the edges of grunerite grains. Stilpnomelane is ubiquitous throughout the area sampled. It occurs as 0.1 mm long individual needles randomly oriented in recrystallized chert bands, and as 0.5 mm long needles and fan-shaped grains. Chlorite is present in most samples, although it appears to be slightly more common in L1N rocks. It occurs as mats of 0.1-1 mm wide grains surrounding quartz +/- carbonate veins. Biotite, grunerite, hornblende and sulfides are frequently contained in the chlorite mats. Chlorite also forms individual isolated 0.1 mm wide grains in recrystallized chert bands. Biotite occurs as 0.2 mm wide tabular, inclusion-free grains within a chlorite mat. Quartz, sulfide, magnetite and zircon inclusions are common in larger grains with embayed margins (Plate 3).

Very fine-grained, thin laminations of graphite are present in many of the samples. The graphite occurs in blocky patches, spatially related to magnetite or sulfides (Plate 4). Magnetite occurs as 0.1-0.5 mm wide subhedral to anhedral grains which commonly coalesce into thin layers. It is typically found

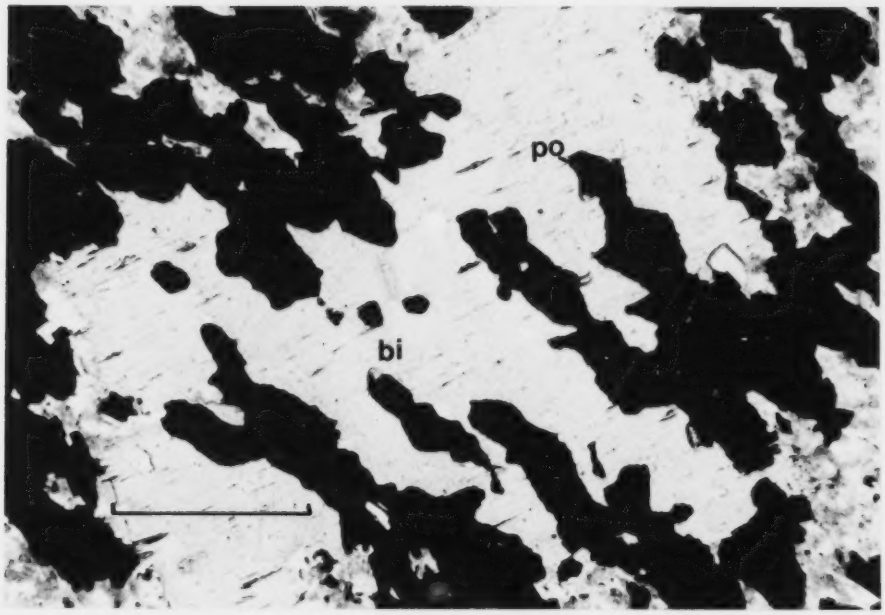

Plate 3. Biotite grain grown around pyrrhotite
Taken in plane-polarized light. Scale bar = 1mm

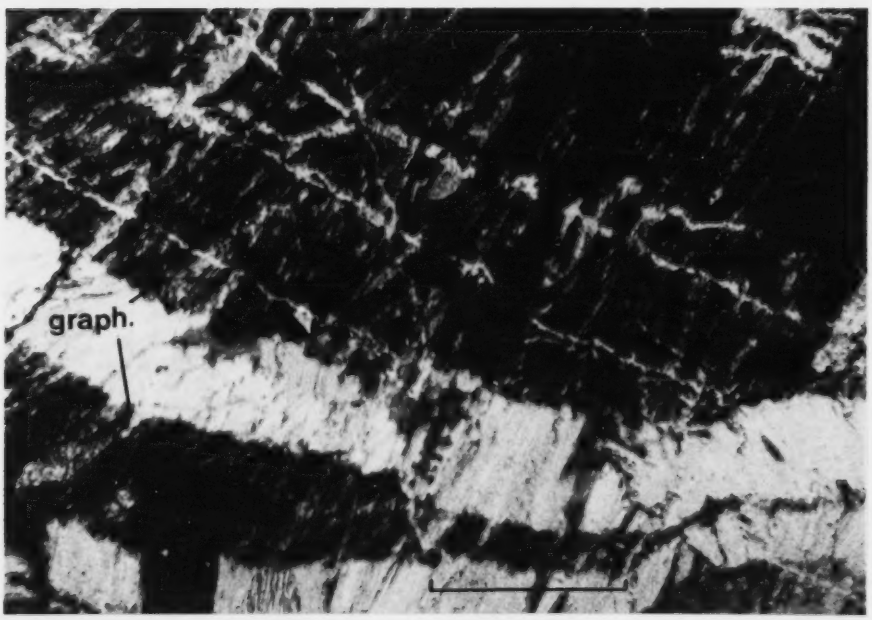

Plate 4. Blocky patches of graphite laminations
Taken in plane-polarized light. Scale bar = 1mm

with grunerite, stilpnomelane and, locally, graphite. In many samples, magnetite grains are rimmed by pyrrhotite (Plate 5), and, locally, magnetite is found as small inclusions within larger pyrrhotite grains.

Pyrrhotite is the most common sulfide noted in the samples. It is generally 0.1-0.5 mm wide, anhedral, and occurs as masses of individual grains interstitial to silicates, rimming or pseudomorphing magnetite, and along grain boundaries in arsenopyrite. Pyrrhotite generally occurs in close proximity to quartz +/- carbonate veins, and is often spatially associated with visible gold when present. Euhedral to subhedral, 0.5-5 mm long arsenopyrite prisms are found adjacent to quartz +/- carbonate veins. Grain boundaries and fractures are often coated with pyrrhotite, and locally pyrrhotite is included within arsenopyrite. Visible gold is frequently spatially associated with arsenopyrite. Anhedral pyrite is occasionally noted in some samples, where it contains, or forms inclusions in, pyrrhotite grains. It is rarely noted as local concentrations of square euhedral grains. Chalcopyrite is a common though relatively minor component of the samples. It occurs as 0.1-0.3 mm wide patches within pyrrhotite grains. Ilmenite is also common though scarce, and forms small individual inclusions within pyrrhotite grains.

Visible gold grains are generally <0.05 mm wide, although some grains were noted up to 0.15 mm in width. It is found in close proximity to quartz +/- carbonate veins, where it occurs as isolated flecks within arsenopyrite or pyrrhotite grains, or more commonly within pyrrhotite along arsenopyrite grain boundaries and fractures (Plate 6).

Petrological Relationships

Well banded, unaltered unmineralized OIF at George Lake represents the closest approximation to the original chemical precipitate. An understanding of the mineralogy of the unmineralized OIF may help to establish the processes leading to its development. Major constituents of the unmineralized OIF include quartz, magnetite, grunerite, stilpnomelane and graphite (organic Carbon) and

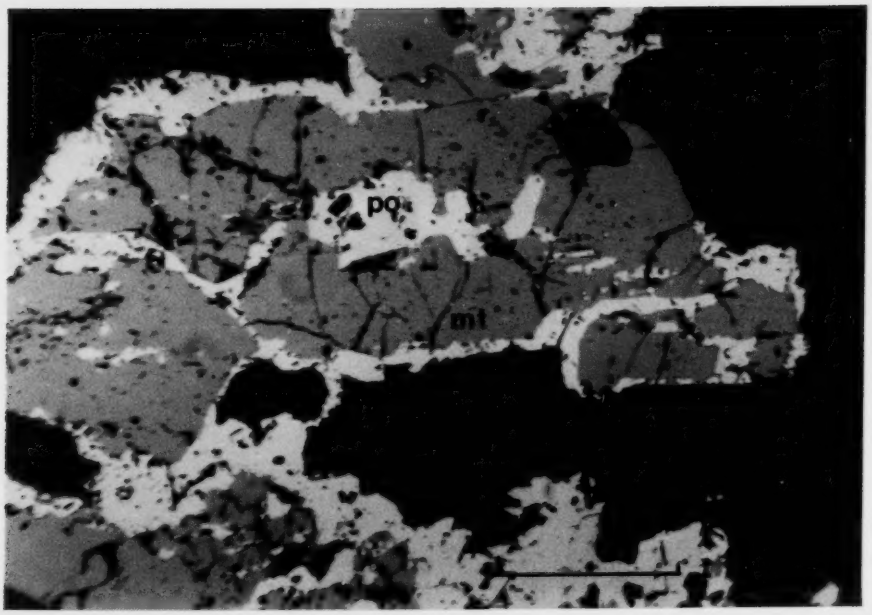

Plate 5. Magnetite grains rimmed with pyrrhotite
Taken in Plain reflective light. Scale bar = 1mm

Plate 6. Visible gold in fracture with pyrrhotite in arsenopyrite
Taken in Plain reflective light. Scale bar = 1mm

minor ferroan calcite. The quartz (recrystallized chert), stilpnomelane and graphite are interpreted to be products of diagenesis of the original OIF, and the magnetite, grunerite and ferroan calcite are interpreted to have formed during low grade metamorphism (Klein 1973).

Magnetite in iron formations can be produced by the following reactions (Ayers 1972, Klein 1973);

$$3\ \text{Siderite} + \tfrac{1}{2}\ O_2 = \text{Magnetite} + 3\ CO_2 \quad \textbf{(1)}$$

$$6\ \text{Hematite} + C_{organic} = 4\ \text{Magnetite} + CO_2 \quad \textbf{(2)}$$

As neither siderite or hematite are present in the unmineralized OIF, it is difficult to identify which, if either, of the above reactions occurred. The CO_2 produced by either of these reactions could subsequently have reacted with Ca and Fe to produce the minor amounts of ferroan calcite noted in the unmineralized OIF (Saager et al. 1987)

Grunerite can be produced from several reactions involving dehydration of early hydrous phases or decarbonatization of original carbonates (Klein 1983, Saager et al. 1987, Hasse 1982, Floran and Papike 1978, Caddey, 1991);

$$\text{Greenalite} + 4\ \text{Quartz} = 2\ \text{Minnesotaite} + 2\ H_2O \quad \textbf{(3a)}$$

$$\text{Minnesotaite} = \text{Grunerite} + 4\ \text{Quartz} + 4\ H_2O\ \text{(dehydration)} \quad \textbf{(3b)}$$

$$7\ \text{Siderite} + 8\ \text{Quartz} + H_2O = \text{Grunerite} + 7\ CO_2\ \text{(decarbonatization)} \quad \textbf{(4)}$$

Again, since siderite, greenalite and minnesotaite are absent from the unmineralized OIF, it is difficult to interpret which reaction was responsible for producing the grunerite.

Several minerals in the OIF at George Lake exhibit textures that indicate their relative positions in a paragenetic sequence. Graphite occurs as very thin laminations that have been mechanically separated into fracture-bound blocks (Plate 4). Other minerals such as grunerite and chlorite, which are interstitial to the graphite laminations, are not disrupted by fractures as the graphite is.

Therefore, although the graphite appears to overprint the interstitial minerals, it must be an early phase, now included as preserved laminations within the later minerals. Groundmass carbonate often contains inclusions of quartz, stilpnomelane, graphite, and magnetite, and must therefore be later than these minerals. Similarly, biotite often contains inclusions of quartz, graphite and pyrrhotite, indicating that it is later than these included minerals. Hornblende rims and pseudomorphs grunerite and must therefore be later than the grunerite. Pyrrhotite has a similar relationship to magnetite, and is therefore later as well. Pyrrhotite, pyrite, and chalcopyrite are interpreted to be coeval since they commonly form inclusions in each other. However, pyrrhotite and pyrite are noted as inclusions in arsenopyrite, and must therefore be earlier than, or coeval with that sulfide.

Unmineralized and Mineralized OIF

From both microscopic and macroscopic observations, it is apparent that unmineralized and mineralized OIF are separated from each other by a transitional zone in which unmineralized OIF grades into mineralized OIF. This has important implications regarding the formation of the ore deposits at George Lake, as it indicates that mineralized OIF is an altered form of unmineralized OIF.

The transition from unmineralized to mineralized OIF, and vice versa, develops as a halo around one or more major (approximately 10 cm or greater) quartz +/- carbonate veins. Similar changes on a smaller scale occur around narrower veins, especially within the transitional zone.

In unmineralized, unaltered OIF, primary banding is well preserved as 0.5-5 mm wide alternating bands of recrystallized chert and silicates + oxides (Plate 7). Chert bands contain fine-grained stilpnomelane needles, grunerite rosettes (locally with ferroan calcite cores), and occasionally fine-grained chlorite. The silicate + oxide bands are composed of randomly oriented grunerite laths, stilpnomelane, graphite, and magnetite blebs. Quartz and carbonate veins, as well as biotite, hornblende, and chlorite, are very rare in

unmineralized OIF. If present, these minerals are found in the silicate + oxide layer, adjacent to a vein. Sulfides are virtually absent from unmineralized OIF.

As a major quartz +/- carbonate vein is approached, numerous changes occur within the unmineralized OIF (Plate 8). The most noticeable change is that the primary banding is virtually obliterated. The original constituents of the unmineralized OIF bands are preserved, but occur in irregular patches, intermixed with each other, as opposed to alternating bands. Several changes in the mineralogy also develop. Grunerite grains become larger and more feathery in appearance. Hornblende is noted at the edges and terminations of these grains, where it replaces the pre-existing grunerite. Grunerite rosettes and graphite laminations become less common, and chlorite, biotite, and quartz +/- carbonate veins increase in abundance. Pyrrhotite becomes a common though minor constituent and forms rims around the magnetite grains (Plate 5). The ratio of pyrrhotite to magnetite increases as the transition advances. The OIF is considered mineralized (Plate 9) when the sulfide content reaches 1% or greater, which generally occurs 2.5-0.5 m away from a major quartz vein. Pyrrhotite is the most abundant sulfide in the mineralized OIF, although pyrite and chalcopyrite occur in minor amounts. As mineralization progresses to the vein, magnetite becomes rare to absent as it is replaced by pyrrhotite. This process of replacement is supported petrographically by the gradual depletion of magnetite and concomitant enrichment of pyrrhotite as it pseudomorphs magnetite. In addition, mineralized OIF exhibits increased abundances of quartz and carbonate veins, hornblende, and chlorite, and the addition of arsenopyrite and gold. Directly adjacent to the major quartz +/- carbonate vein, chlorite, quartz, pyrrhotite, arsenopyrite and gold predominate.

Paragenetic Sequence

The petrological relationships described earlier, combined with the observed transitional changes described above, have led to the establishment of the following paragenetic sequence for the OIF at George Lake. Quartz, stilpnomelane and graphite are products of the diagenesis of the original

Plate 7. Unmineralized OIF

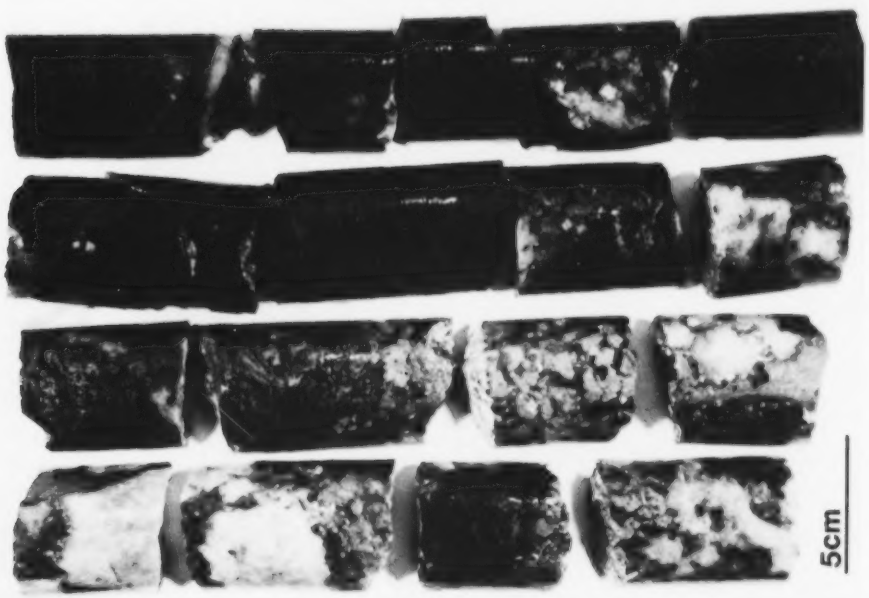

Plate 8. Transition from unmineralized to mineralized OIF

Plate 9. Mineralized OIF

chemical precipitate. Dehydration and decarbonatization reactions between these, and other now absent minerals produced magnetite, grunerite and groundmass carbonate. These minerals, together with quartz, stilpnomelane and graphite, constitute the well banded, unmineralized and unaltered OIF. Subsequent alterations to this mineral assemblage are due to fluids introduced to the OIF at some time after its formation, which formed the quartz +/- carbonate veins. Hornblende formed at the edges and terminations of grunerite grains, and chlorite halos formed around the veins. Coeval with, and possibly subsequent to hornblende development, pyrite, pyrrhotite, chalcopyrite, biotite, arsenopyrite and gold were deposited.

Genetic Model for Gold Deposition at George Lake

The association of gold with sulfides adjacent to quartz veins, together with the non-stratiform nature of this mineralization, preclude a syngenetic model for gold deposition at George Lake. The criteria established earlier, to discriminate between modified syngenetic and epigenetic gold deposition, must now be applied to the results of the petrographic study.

Gold concentrations are relatively low in the unmineralized OIF (Chandler and Holmberg 1990), which is typically located outside of the ore zones surrounding quartz veins. As unmineralized OIF is common at George Lake, both laterally on strike with, and stratigraphically above mineralized OIF, it is difficult to envision a modified syngenetic process of gold deposition.

Pyrrhotite is clearly a secondary mineral, as indicated by its appearance and abundance adjacent to quartz veins, and by its documented replacement of magnetite. Following the suggestion by Groves et al. (1987) that sulfides and gold are synchronous, the gold at George Lake can not be primary, and hence a modified syngenetic origin is insupportable.

The deposition of gold at George Lake must therefore be a result of epigenetic processes, and more specifically, the result of a sulfidation reaction. This process is discussed in the following chapter.

CHAPTER 4
PROCESSES OF GOLD DEPOSITION

Sulfidation

Epigenetic gold deposits require the introduction of gold from an external source, via hydrothermal fluids, to a favourable horizon, and the subsequent precipitation of gold from the fluids. Sulfidation reactions represent a chemical process by which this precipitation may occur. This type of reaction has been suggested as a means of gold deposition in volcanogenic massive sulfide deposits (Hannington and Scott 1989), as well as banded iron formation-hosted gold deposits (Phillips et al. 1984, Macdonald and Fyon 1986), and is interpreted to be the process by which gold was deposited in iron formation at George Lake.

In sulfur-rich, low temperature fluids (up to 350°C), gold is transported primarily as the bisulfide complex $HAu(HS)_2$ (Seward 1984, Hannington and Scott 1989, Phillips et al. 1984). The stability of this complex in a hydrothermal fluid is dependent on the temperature, pH, reduced sulfur concentration, and oxidation or sulfidation state of the fluid (Seward 1984, Hannington and Scott 1989). In order for gold to precipitate, changes to one or more of these fluid conditions must occur. If the temperature of the solution is decreased to below about 150°C, the solubility of the bisulfide complex decreases, prompting gold to precipitate (Hannington and Scott 1989). Secondly, a decrease in the reduced sulfur concentration will cause the bisulfide complex to destabilize and gold to precipitate.

Phillips et al. (1984) propose the following sulfidation reactions for the deposition of gold in banded iron formation;

$$FeO_{(silicates)} + HAu(HS)_2 + 1/4\ O_2 = FeS_2 + 3/2\ H_2O + Au \quad (5)$$

$$Fe_3O_4 + 3\ HAu(HS)_2 + 1/4\ O_2 = 3\ FeS_2 + 9/2\ H_2O + 3\ Au \quad (6)$$

$$2\ Fe_3O_4 + 3\ HAu(HS)_2 = 6\ FeS + 9/2\ H_2O + 7/4\ O_2 + 3\ Au \quad (7)$$

In addition to these, the following reaction may also have been significant in the deposition of gold at George Lake;

$$2\ FeO_{(silicates)} + HAu(HS)_2 = 2\ FeS + 3/2\ H_2O + 1/4\ O_2 + Au \quad \textbf{(8)}$$

In these four reactions, the precipitation of iron sulfides and gold is prompted by a decrease in the reduced sulfur concentration. In reactions (5) and (6), this decrease is a result of oxidation of the bisulfide complex. Reactions (7) and (8) however, do not involve oxidation. Destabilizing of the bisulfide complex in these cases is a result of reaction between the fluid carrying the complex, and the rock it infiltrates, causing the transfer of iron from an oxide or silicate to the sulfide. Whether a result of oxidation or disequilibrium between reactants, reactions (5) to (8) show that destabilization of the bisulfide complex will lead to the precipitation of iron sulfides and gold.

At George Lake, the abundance of pyrrhotite and relative paucity of pyrite suggest that reactions (5) and (6) did not occur to a significant degree. The close association between magnetite and pyrrhotite implies that reaction (7) may have been responsible for the deposition of gold in the OIF. This does not preclude the possibility that reaction (8) occurred as well. To test whether or not iron silicates were involved in a sulfidation reaction, the composition of numerous grunerite samples was examined. The results of this study are reported below.

Mineral Chemistry

Sulfidation is an important process in the formation of epigenetic gold deposits in iron-rich host rocks. It is interpreted to have played a significant role in the deposition of gold in banded iron formation in the Yilgarn Block, Western Australia (Phillips et al. 1984, Groves et al. 1987), in the Geraldton (Macdonald and Fyon 1986, Macdonald 1983) and Lupin camps (Lhotka 1988, Lhotka and Nesbitt 1989) and at George Lake.

In the previous section, four sulfidation reactions were presented. Each

reaction requires a source of iron, which reacts with a bisulfide complex to produce iron sulfides, thereby destabilizing the complex and prompting the deposition of gold. According to these reactions, iron is provided by iron silicate and/or iron oxide. At George Lake, both iron silicates (grunerite) and iron oxides (magnetite) are abundant, and may have played a role in the sulfidation process. The documented replacement of magnetite by pyrrhotite in OIF at George Lake strongly suggests that reaction (7) was significant in the sulfidation process. However, since grunerite is present as well in the OIF at George Lake, reaction (8) may also have occurred. This possibility was tested by determining the composition of grunerites from George Lake OIF.

Microprobe analyses were conducted on grunerites from both unmineralized and mineralized OIF. The premise of this investigation was that participation by grunerites in a sulfidation reaction should be reflected as variations in their iron content. Specifically, grunerites from unmineralized OIF should be more iron-rich than those from mineralized OIF, if grunerite was a source of iron for sulfidation, and reaction (8) occurred.

The X_{Fe} (defined as Fe/(Fe+Mg)) of grunerite, $(Fe,Mg)_7Si_8O_{22}(OH)_2$, can range from approximately 0.30 (the Mg-end member cummingtonite) to 1 (the pure Fe-end member grunerite) (Deer et al. 1985), and is a measure of the relative abundance of Fe occupying the (Fe,Mg) site. Thus, a comparison of the X_{Fe} of grunerites from mineralized and unmineralized OIF tests whether grunerite was involved in sulfidation processes at George Lake.

Representative grunerite microprobe analyses are presented in Tables 1 and 2, including the X_{Fe} calculated for each sample. (Complete results are presented in Appendix 2). The ratio of Fe to Mg in each sample can be represented by plotting the stoichiometric values of these elements. In Fig. 7 the stoichiometric values of Fe and Mg from representative grunerite microprobe analyses, given in Tables 1 & 2, are plotted. The random scatter of the data points on this graph, with no apparent clustering of data points, indicates that stoichiometrically, grunerites from unmineralized OIF are similar to those from mineralized OIF.

Sample	BH2047	BH2033	BH2029	BH2075A	BH1037	BH1004B-1	BH1073B	BH1073A
Type	UM	UM	UM	UM	UM	UM	UM	UM
Mineral	GRU	GRU	GRU	GRU	GRU	GRU	GRU	GRU
SiO2	50.73	50.05	49.39	50.08	50.07	49.94	51.36	50.39
TiO2	0.00	0.02	0.02	0.03	0.00	0.00	0.03	0.00
Al2O3	0.47	0.35	0.19	0.25	0.20	0.31	0.07	0.11
FeO	40.70	41.71	41.38	42.36	41.33	42.45	40.57	41.67
MnO	0.03	0.07	0.04	0.10	0.10	0.10	0.19	0.06
MgO	6.53	4.82	6.15	5.06	5.45	4.91	6.43	5.50
CaO	0.54	0.40	0.29	0.43	0.25	0.30	0.20	0.17
Na2O	0.09	0.02	0.02	0.04	0.09	0.09	0.05	0.10
K2O	0.00	0.00	0.00	0.00	0.00	0.00	0.00	0.00
Total	99.09	97.43	97.47	98.35	97.48	98.09	98.89	98.00
Cations based on 23 O								
Si	7.9503	8.0326	7.9285	7.9880	8.0184	7.9915	8.0461	8.0284
Ti	0.0000	0.0020	0.0019	0.0032	0.0000	0.0000	0.0036	0.0000
Al	0.0873	0.0661	0.0363	0.0471	0.0375	0.0577	0.0130	0.0211
Fe	5.3339	5.5971	5.5543	5.6498	5.5350	5.6799	5.3140	5.5524
Mn	0.0035	0.0094	0.0049	0.0129	0.0134	0.0134	0.0247	0.0084
Mg	1.5256	1.1528	1.4715	1.2038	1.3012	1.1706	1.5016	1.3054
Ca	0.0912	0.0683	0.0501	0.0738	0.0421	0.0520	0.0328	0.0297
Na	0.0267	0.0061	0.0061	0.0113	0.0287	0.0272	0.0146	0.0294
K	0.0000	0.0000	0.0000	0.0000	0.0000	0.0000	0.0000	0.0000
Sum	15.0185	14.9344	15.0536	14.9899	14.9763	14.9923	14.9504	14.9748
Fe/(Fe+Mg)	0.7776	0.8292	0.7906	0.8244	0.8097	0.8291	0.7797	0.8096

UM = unmineralized, GRU = grunerite

Table 1. Representative microprobe analyses of grunerites from unmineralized OIF

Sample	BH2036B	BH2030B-2	BH2030B-2	BH2030B-1	BH2030A	BH2031C	BH2031C	BH2031A
Type	MIN	MIN	MIN	MIN	MIN	MIN	MIN	MIN
Mineral	GRU	GRU	GRU	GRU	GRU	GRU	GRU	GRU
SiO2	49.70	48.73	49.71	49.72	50.87	50.93	49.09	49.61
TiO2	0.01	0.02	0.05	0.02	0.00	0.00	0.01	0.03
Al2O3	0.37	0.24	0.02	0.36	0.31	0.22	0.32	0.18
FeO	42.15	43.09	43.12	41.32	39.69	41.54	41.75	41.62
MnO	0.10	0.24	0.21	0.22	0.28	0.31	0.25	0.16
MgO	5.51	4.67	4.94	5.10	5.94	6.22	6.02	4.95
CaO	0.30	0.27	0.39	0.38	0.27	0.37	0.27	0.39
Na2O	0.11	0.10	0.00	0.07	0.11	0.02	0.09	0.07
K2O	0.00	0.00	0.00	0.00	0.00	0.00	0.00	0.00
Total	98.26	97.36	98.61	97.19	97.47	99.61	97.81	97.02
Cations based on 23 O								
Si	7.9348	7.9200	7.9470	8.0013	8.0710	7.9718	7.8818	8.0128
Ti	0.0012	0.0027	0.0056	0.0025	0.0000	0.0000	0.0018	0.0037
Al	0.0702	0.0459	0.0381	0.0683	0.0572	0.0407	0.0610	0.0340
Fe	5.6271	5.8566	5.7646	5.5595	5.2660	5.4364	5.6057	5.6214
Mn	0.0134	0.0326	0.0284	0.0298	0.0381	0.0415	0.0334	0.0225
Mg	1.3117	1.1319	1.1768	1.2243	1.4042	1.4511	1.4416	1.1915
Ca	0.0521	0.0473	0.0669	0.0650	0.0467	0.0623	0.0462	0.0680
Na	0.0347	0.0326	0.0000	0.0208	0.0323	0.0063	0.0267	0.0233
K	0.0000	0.0000	0.0000	0.0000	0.0000	0.0000	0.0000	0.0000
Sum	15.0452	15.0696	15.0274	14.9715	14.9155	15.0101	15.0982	14.9772
Fe/(Fe+Mg)	0.8110	0.8380	0.8305	0.8195	0.7895	0.7893	0.7954	0.8251

MIN = mineralized, GRU = grunerite

Table 2. Representative microprobe analyses of grunerites from mineralized OIF

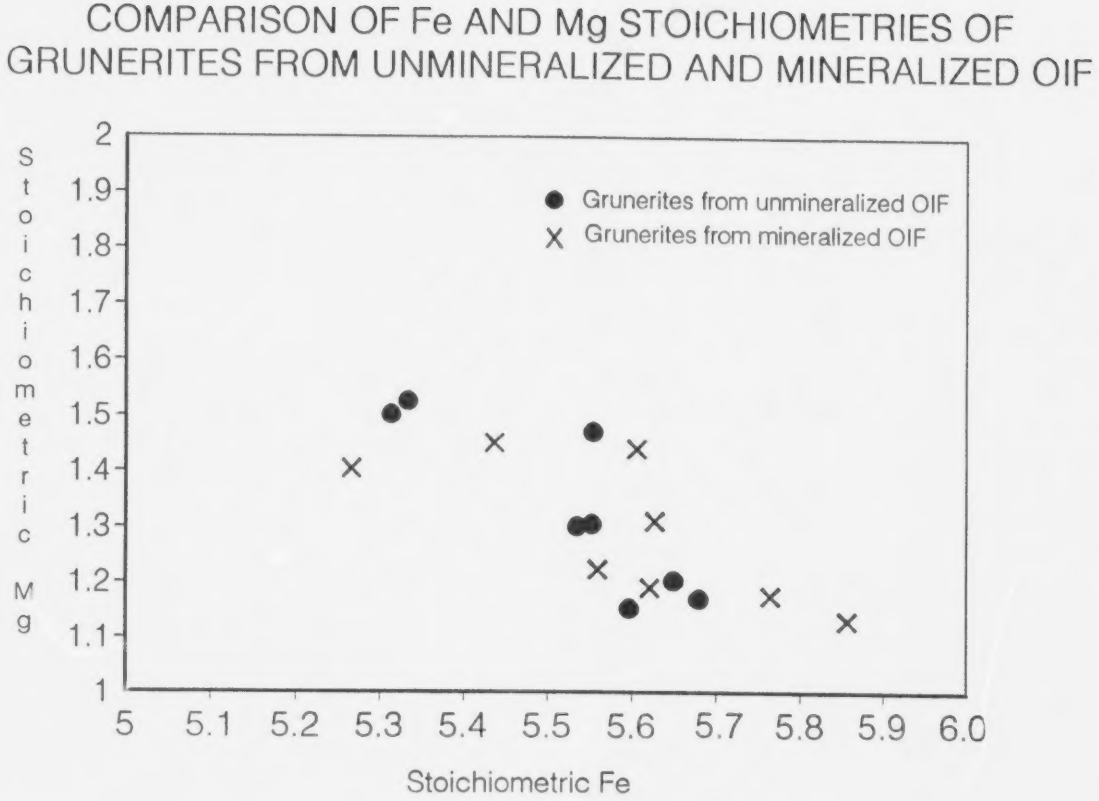

Fig. 7. Stoichiometric values of Fe versus Mg

Histograms of X_{Fe} values of grunerites from unmineralized and mineralized OIF were tabulated from the complete data set (Appendix 2) and are presented in Figs. 8 and 9 respectively. The X_{Fe} values of the grunerites from unmineralized OIF range from 0.72 to 0.86 and average 0.80 +/- 1σ. For grunerites from mineralized OIF, the X_{Fe} values range from 0.74 to 0.84, and average 0.81 +/- 1σ. These histograms clearly show that the range in X_{Fe} values, as well as the average X_{Fe} values, are similar, regardless of whether the grunerites came from unmineralized or mineralized OIF.

If grunerite was involved in the sulfidation process at George Lake, and reaction (8) had occurred, both the ratio of Fe:Mg, and the ratio of Fe/(Fe+Mg) should be affected. A clear distinction would exist between the mineral chemistry of grunerites from unmineralized OIF and those from mineralized OIF. The ratio of Fe:Mg from unmineralized samples would be greater than the ratio in mineralized samples. Fig. 7 clearly shows a random scatter of data points, with no distinction based on degree of mineralization. As well, if reaction (8) occurred, grunerites from unmineralized OIF would have a higher X_{Fe} than grunerites from mineralized OIF, since iron from the grunerites would have been consumed in the reaction. Microprobe analyses of grunerites from both types of OIF, show that there is no variation in the X_{Fe} of grunerites, regardless of their accompanying sulfide abundance. Consequently, reaction (8) is interpreted to have been insignificant in the sulfidation process at George Lake. The primary, if not exclusive, source of iron for sulfidation of the OIF is interpreted to have been magnetite.

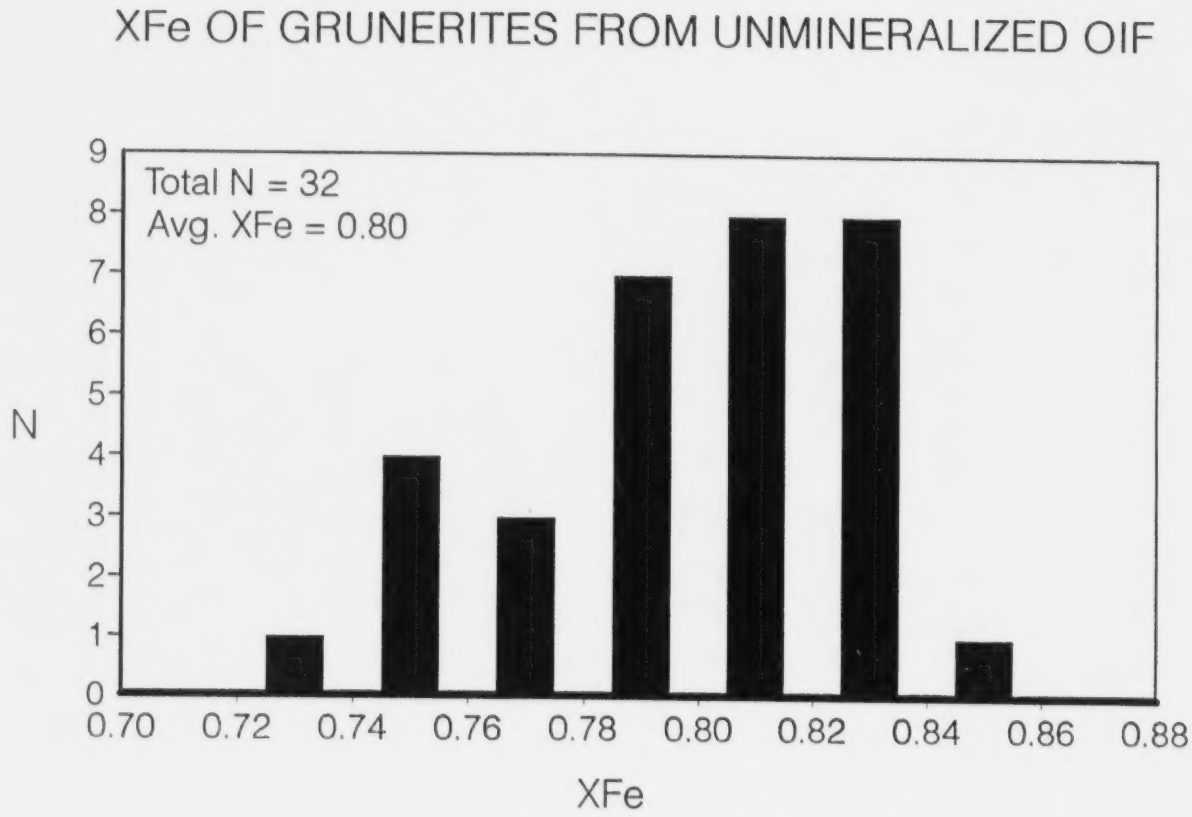

Data from complete microprobe analyses (Appendix 2)

Fig. 8. Histogram of X_{Fe} values of grunerites from unmineralized OIF

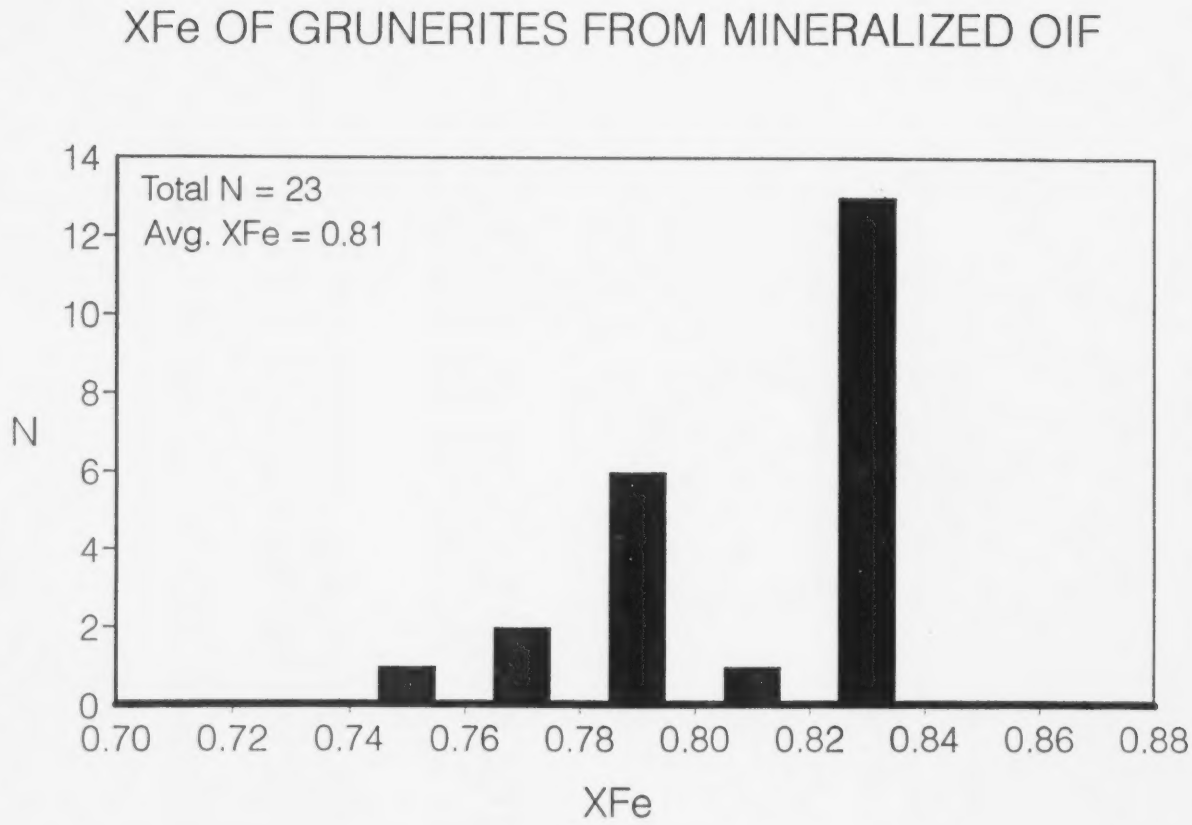

Data from complete microprobe analyses (Appendix 2)

Fig. 9. Histogram of X_{Fe} values of grunerites from mineralized OIF

CHAPTER 5
DISCUSSION

Currently, three models have been proposed for the deposition of gold in banded iron formation; a syngenetic model, in which gold is primary, a modified syngenetic model, in which gold is primary but later remobilized, and an epigenetic model in which gold is secondary, having been introduced to the iron formation by hydrothermal fluids. At George Lake, gold is interpreted to have been deposited by epigenetic processes, based on the association of gold and sulfide mineralization with quartz veins, the non-stratiform nature of the mineralization, and relatively low gold values away from the quartz veins.

Sulfidation reactions represent a means of epigenetic gold deposition and have been suggested for volcanogenic massive sulfide deposits (Hannington and Scott 1989) as well as for banded iron formation-hosted gold deposits (Lhotka 1988, Phillips et al. 1984). This process involves the introduction of gold-bearing hydrothermal fluids to an iron-rich rock, and the subsequent deposition of both sulfide minerals and gold. Of the four sulfidation reactions presented earlier, the following two reactions were deemed possible at George Lake, based on the petrology of the OIF;

$$2\ Fe_3O_4 + 3\ HAu(HS)_2 = 6\ FeS + 9/2\ H_2O + 7/4\ O_2 + 3\ Au \qquad \textbf{(7)}$$

$$2\ FeO_{silicate} + HAu(HS)_2 = 2\ FeS + 3/2\ H_2O + 1/4\ O_2 + Au \qquad \textbf{(8)}$$

The observed replacement of magnetite by pyrrhotite strongly suggests that reaction (7) played a significant role in the sulfidation process at George Lake. Microprobe analyses of grunerites from both unmineralized and mineralized OIF was conducted to evaluate whether or not grunerite participated in the sulfidation process as well, according to reaction (8). To make this assessment, the X_{Fe} values (Fe/(Fe+Mg)) of grunerites were calculated from the microprobe analyses, and histograms showing the distribution of these values were plotted. Figs. 8 and 9 show the X_{Fe} histograms for grunerites from

unmineralized and mineralized OIF respectively. Had grunerite participated in sulfidation according to reaction (8), a loss of Fe from grunerites upon mineralization of the OIF would be expected. This would be reflected as X_{Fe} values for grunerite from mineralized OIF lower than those from unmineralized OIF. Comparison of Figs. 8 and 9 shows that the range in grunerite X_{Fe} values, as well as the average grunerite X_{Fe} values are similar for both unmineralized and mineralized OIF. These results indicate that there was no quantifiable loss of iron from grunerite coincident with mineralization, and it is therefore interpreted that grunerite was not an active participant in the sulfidation process at George Lake.

Reaction (8) shows that the iron necessary for sulfidation may be supplied by iron silicates contained in the host rock. Four iron silicate minerals are present in the OIF at George Lake; grunerite, hornblende, chlorite and stilpnomelane. Grunerite is considered the most likely of these minerals to have participated in reaction (8) because of its abundance in OIF at George Lake, and because it has been shown to have been significant in the sulfidation of unmineralized iron formation at the Lupin deposit (Lhotka 1988). As stated earlier, hornblende and chlorite are common in the mineralized OIF. Although these minerals are also present in the unmineralized OIF (according to its definition as having nil to trace sulfides), they are restricted to parts of the unmineralized OIF that are transitional to mineralized OIF, and which appear to be altered. The potential reactants in reaction (8) must have been present in the well-banded, unaltered, unmineralized OIF. As only rare hornblende and chlorite were noted in this unaltered OIF, they are not considered abundant enough to have contributed the amount of iron required for the sulfidation observed. Stilpnomelane, like grunerite, is common in the well-banded, unaltered, unmineralized OIF. Two varieties of stilpnomelane are known, based on the oxidation state of iron in the mineral; ferristilpnomelane contains abundant Fe^{3+}, and ferrostilpnomelane contains mainly Fe^{2+}. The petrographic properties of these two varieties of stilpnomelane are markedly different (Deer et al. 1985). From petrographic observations, as well as microprobe analysis

(Appendix 2), stilpnomelane in both the unmineralized and mineralized OIF at George Lake is confirmed to be ferristilpnomelane. A change in the ratio of Fe^{3+}:Fe^{2+}, as a result of participation by ferristilpnomelane in reaction (8), would likely be accompanied by petrographic changes as the ferristilpnomelane became relatively more Fe^{2+}-rich. In fact, no petrographic evidence exists in the OIF to suggest that stilpnomelane participated in reaction (8).

As documented by the results given above, as well as the results of the microprobe analyses of grunerites, it is apparent that none of the iron-rich silicates present in the OIF at George Lake were reactants in reaction (8). Sulfidation is therefore interpreted to have been a result of reaction (7), with magnetite as the exclusive source of iron.

Mineral Equilibria in the FeO-FeS System

In order to better understand the dynamics of the sulfidation process at George Lake, and to refine a model for the deposition of gold in the OIF, a mineral stability field diagram for the FeO-FeS system was constructed (Fig. 10). As equilibrium reactions between iron oxides and iron sulfides are dependent upon oxygen and sulfur fugacities, the mineral stability fields were plotted in this diagram as functions of fO_2 and fS_2. In addition, reaction equilibria between grunerite and magnetite and grunerite and pyrrhotite were plotted as contours of X_{Fe}(grunerite). For the construction of Fig. 10, thermodynamic data for grunerite were obtained from Holland and Powell (1990), and data for all other minerals were taken from Robie et al. (1979). Calculations of reaction equilibria involving grunerite assumed a change in heat capacity as a result of reaction equal to 0 ($\Delta Cp_{(reaction)} = 0$). An enlargement of the portion of Fig. 10 applicable to George Lake is presented in Figs. 11 and 12.

As no direct measurements were made of the temperature of pressure of the fluids involved in mineralization at George Lake, it was necessary to estimate these conditions. A temperature of 600 K (327° C) and a pressure of 2 kbars were assumed to be appropriate. This estimation is based on the stability regimes of those minerals produced as a result of mineralization

(namely hornblende and chlorite), and on well-documented estimates of temperature and pressure of fluids related to Archean gold deposition in both lode gold (Colvine et al. 1988), and banded iron formation-hosted deposits (Groves et al. 1987, Groves et al. 1988). It should be noted, that variations of +/- 50° C in the temperature estimates used to construct Fig. 10 will alter the positions of the equilibria reaction lines, although the interpretations based on this figure will still apply. Changes to the pressure estimate of 1-2 kbars will not result in significant changes to Fig. 10.

Interpretation of the Sulfidation Process based on Mineral Stabilities and Reaction Equilibria

As stated earlier, the mineral stability fields and reaction equilibria shown in Figs. 10 and 11 can be used to gain a more comprehensive understanding of the sulfidation process at George Lake. The following discussion will centre on the relationship between the grunerite compositions, determined from microprobe analyses and reported earlier, and the chemistry of the fluids which were responsible for sulfidation of the OIF at George Lake. Two assumptions were necessary in order to form the interpretations which follow. First, it is assumed that chemical equilibrium existed between the mineral and vapour phases present in the unmineralized OIF, and as such, the composition of grunerites, as established by microprobe analysis, is representative of the unmineralized OIF as a whole. Second, the effect of fluids on the OIF, represented by the documented alteration halos surround quartz veins in mineralized OIF, is assumed to be a result of high water-rock ratios immediately adjacent to the veins, and lower water-rock ratios away from the veins. This implies that the alteration of OIF adjacent to quartz veins was a result of reactions between the fluid and the rock, where the chemistry of the infiltrating fluid was dominant. Away from veins, where the water-rock ratio was lower, the rock was not significantly altered by the fluids. With these assumptions in mind, the following interpretations can be made about the sulfidation process at George Lake.

Fig.10

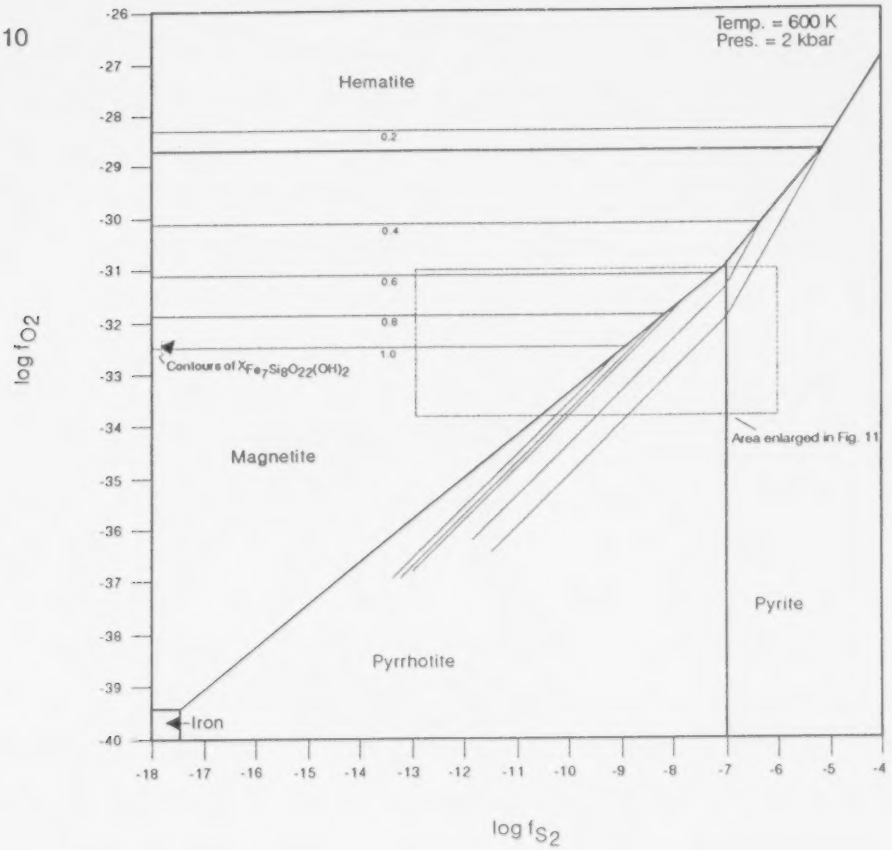

Fig. 11

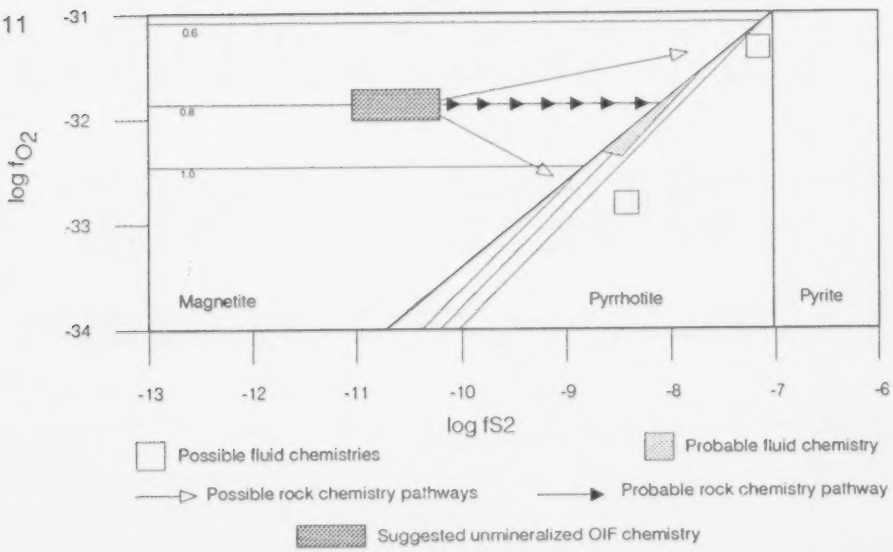

Fig. 10. Log fO_2 vs. log fS_2 diagram for the FeO-FeS system at 600 K and 2kbars with contours of X_{Fe} of grunerite
Fig. 11. Enlargement of Fig. 10 for region of interest at George Lake

The evidence presented in this study strongly suggests that gold and sulfides in the OIF at George Lake were precipitated from fluids which infiltrated the unmineralized OIF. Prior to the introduction of fluids, all of the OIF was unmineralized. Mineralized OIF therefore represents, in effect, chemically altered unmineralized OIF. From petrographic and microprobe analyses, and using Figs. 10 and 11, the oxygen and sulfur fugacities of unmineralized and mineralized OIF can be determined. Microprobe analyses of grunerites from unmineralized OIF, as represented in Fig. 8, show that the range in X_{Fe} values is 0.72 to 0.86, with an average X_{Fe} of 0.80 +/- 1σ. Contours of X_{Fe}(grunerite), representing equilibrium lines for the reaction between grunerite and magnetite, were plotted on Figs. 10 and 11. As grunerite is assumed to be represent the unmineralized OIF as a whole, the oxygen fugacity of this unit can be determined to be $10^{-31.6}$ to $10^{-32.0}$ (Fig. 11). Due to the absence of sulfide phases, the sulfur fugacity of the unmineralized OIF can not be accurately estimated. However, the fS_2 can not be greater than $10^{-8.2}$ to be in equilibrium with OIF in the magnetite stability field, with an X_{Fe}(grunerite) of 0.80. The unmineralized OIF rock chemistry is shown on Fig. 11, although it is noteworthy that since an accurate estimation of the fS_2 can not be made, the representative box in Fig. 11 can potentially fall anywhere along the 0.80 contour line in the magnetite stability field.

According to the sulfidation process, and reactions (7) and (8), upon infiltration of gold- and sulfur-bearing hydrothermal fluids to the OIF, those parts of the OIF adjacent to the fluid conduits were altered, and their fO_2 and fS_2 shifted to become equilibrated with the fluid. Since this alteration involved the precipitation of sulfide minerals, it is reasonable to conclude that the fluids had a higher fS_2 than the unmineralized OIF. In addition, since pyrrhotite and not pyrite was produced, the fS_2 of the fluids must have been within the pyrrhotite stability field. There are three possibilities for the oxygen fugacity of the fluids; an fO_2 greater than, equal to, or less than that of the OIF. Had the log fO_2 of the fluid been either greater or less than that of the OIF (Fig. 11), a shift in the chemistry of the OIF in order to equilibrate with the fluid would have resulted in

a shift in X_{Fe} values of the grunerites to either higher or lower values. Since no shift in the X_{Fe} values of grunerites accompanied sulfidation, the fO_2 of the fluid is interpreted to have been approximately equal to that of the unmineralized OIF. Upon infiltration of the mineralizing fluids, reaction between the fluid and the rock occurred, such that sulfur was added to the OIF, resulting in a shift in the log fS_2 of the rock. Since the fluid and rock oxygen fugacities were in approximate equilibrium, the fO_2 of the rock was not altered. The addition of sufficient sulfur to the unmineralized OIF eventually resulted in the formation of pyrrhotite from magnetite, according to sulfidation reaction (7). This caused the destabilization of the gold-bisulfide complex and the deposition of gold concomitant with pyrrhotite production. Since the water-rock ratio appears to have been high, it is likely that the production of pyrrhotite was limited by the amount of magnetite present in the OIF, and not from the availability of sulfur- and gold-bearing fluids. Again, the lack of a shift in the X_{Fe} values as a result of sulfidation, helps to define the fluid chemistry even further. The X_{Fe} contours representing reaction equilibria between grunerite and pyrrhotite have steep slopes in the pyrrhotite stability field. Had the fluid fS_2 been substantially greater or less than approximately $10^{-8.1}$ (Fig. 11), a shift in the grunerite X_{Fe} would have taken place in the mineralized OIF. Since such a shift is not observed, the fluid chemistry, in terms of sulfur and oxygen fugacities, can be defined, and is shown schematically as the pale shaded box in Fig. 11.

As mentioned previously, the OIF at George Lake is stratigraphically underlain by a silicate iron formation (SIF) bed. This unit consists of abundant chert and grunerite, but contains no appreciable magnetite, sulfides or gold mineralization (Chandler and Holmberg 1990). Gold-bearing fluids likely infiltrated the SIF as well as the OIF, but sulfidation of the SIF did not occur. Microprobe analyses of grunerites from the SIF were not conducted. However, the fluid fO_2-fS_2 conditions were likely in equilibrium with the SIF grunerites, as well as those from the OIF, and sulfidation according to reaction (8) was impeded. A paucity of magnetite in the SIF is interpreted to be the primary reason for no significant gold deposition in that unit.

It should be noted that sulfidation reaction (7), although conceptually valid, would produce an excess amount of oxygen relative to the amount present in the unmineralized OIF. A means of either fixing or removing the excess oxygen would be required for this reaction to proceed. There are numerous possible means of accomplishing this. Since graphite is present in the unmineralized OIF, the excess oxygen could be fixed as CO_2 by the reaction;

$$C + O_2 = CO_2 \qquad (9)$$

However, this reaction would result in a notable decrease in the amount of graphite present in the OIF upon mineralization, which was not documented. Another potential method of fixing the excess oxygen is through the production of SO_2. Abundant reduced sulfur would have been introduced to the unmineralized OIF as bisulfide complexes in the infiltrating fluids. When oxygen was produced in reaction (7), some of the sulfur from the bisulfide complex may have been oxidized according to the reaction;

$$S + O_2 = SO_2 \qquad (10)$$

However, this reaction would likely produce sulphate minerals, none of which were noted in the OIF at George Lake. A third possibility is the production of magnetite from grunerite;

$$3\ Fe_7Si_8O_{22}(OH)_2 + 7/2\ O_2 = 7\ Fe_3O_4 + 24\ SiO_2 + 3\ H_2O \qquad (11)$$

This reaction would produce abundant magnetite at the expense of grunerite and may be preserved as a magnetite-rich, grunerite-poor phase of unmineralized OIF. Variabilities in the magnetite and grunerite content do exist in the OIF, and this method of fixing the excess oxygen may be valid. Further work is required however, to assess this possibility (see Recommendations). A final possibility is that the excess oxygen produced in reaction (7) was not fixed as a mineral or vapour phase, but was carried away by the fluids. This would require a fluid flux exceeding the rate of oxygen production, and may be difficult to evaluate.

Comparison of George Lake to the Lupin Deposit

The Lupin mine, a major banded iron formation-hosted gold deposit in the central Slave Province, provides an interesting example for comparison with the George Lake deposit. At Lupin, located 175 km to the west of George Lake, gold is contained in quartz-veined, silicate- and sulfide-rich iron formation (Lhotka and Nesbitt 1989). This deposit has been the subject of several studies (Kerswill 1984, Kerswill 1992, Lhotka 1988, Lhotka and Nesbitt 1989, and others), although the genesis of the deposit remains a subject of controversy. Kerswill (1984) and Padgham (1992) contend that Lupin is a modified syngenetic deposit, based on the continuity of the ore zone, the abundant sulfide mineralization throughout the deposit, and the relative lack of unmineralized oxide-facies iron formation. They attribute the noted association of gold mineralization with quartz veins as later remobilization of some of the originally syngenetic gold. Lhotka (1988) and Lhotka and Nesbitt (1989) suggest that the Lupin deposit, in addition to numerous similar smaller-scale gold occurrences in the region, are a result of epigenetic sulfidation processes. They contend that unmineralized iron formation does exist at the mine, and base their conclusion on the close association of gold mineralization with quartz veins, and the change in the mineral chemistry, with mineralization, of amphiboles in the deposit.

Microprobe analyses from the Lupin deposit show that grunerite and hornblende from unmineralized iron formation tend to have X_{Fe} values between 0.88 and 0.98, and those from mineralized iron formation range from 0.80 to 0.86 (Lhotka 1988). From these data, Lhotka (1988) concludes that amphiboles took part in sulfidation reactions, which led to the deposition of gold at the Lupin deposit. The observations of Lhotka (1988) differ from those made in this study, in that at Lupin, sulfidation of amphiboles led to the deposition of gold. At George Lake, amphiboles (grunerite) were shown to have been insignificant in the sulfidation process, with magnetite being the source of iron for sulfidation.

It is not the aim of this discussion to evaluate the findings of Lhotka (1988) but rather to fit them into a similar context to George Lake, for the

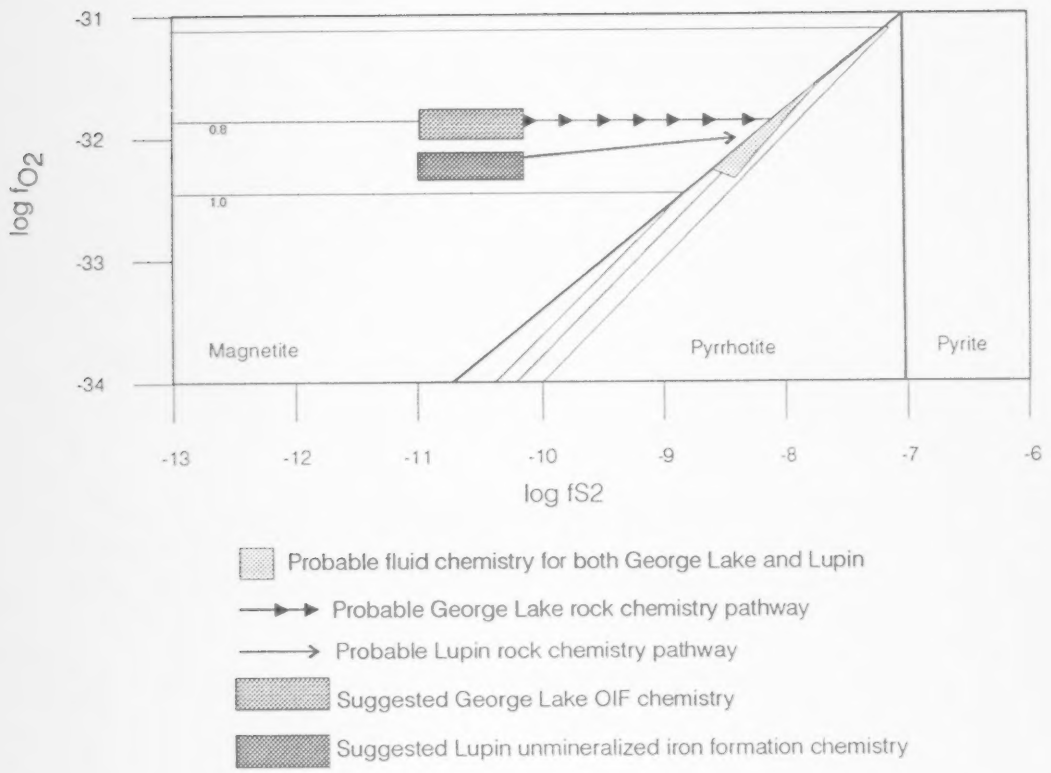

Fig. 12. Possible relationship between Lupin and George Lake rock chemistry pathways.

purposes of comparison. The amphibole X_{Fe} values obtained from Lupin are greater than those from George Lake, indicating that the amphiboles in unmineralized iron formation at Lupin are more iron-rich than those at George Lake. Assuming a similar fluid chemistry for both areas (although this is not necessary for the following interpretation), it is apparent that the amphiboles at Lupin were not in equilibrium with the hydrothermal fluids (Fig. 12). This resulted in a reaction between the amphiboles at the sulfur- and gold-bearing fluids, and the subsequent deposition of gold. It appears as though gold deposition at Lupin was reliant upon, among other thing, the presence of iron-rich amphiboles, in disequilibrium with gold-bearing hydrothermal fluids, while at George Lake, since grunerites were in equilibrium with the fluids, gold deposition was dependent on the presence of magnetite.

CHAPTER 6
CONCLUSIONS AND RECOMMENDATIONS

Conclusions

There are currently three models in circulation for the deposition of gold in banded iron formation; 1) a syngenetic model, in which gold is an original constituent of the iron formation, 2) a modified syngenetic model, in which primary gold is later remobilized, and 3) an epigenetic model, in which gold is introduced to the iron formation by hydrothermal fluids. Syngenetic processes of gold deposition in banded iron formation require that the gold be confined to, and homogenously distributed throughout, the iron formation. At George Lake, gold-bearing zones are stratabound in the OIF, but are not continuous throughout the unit. In fact, gold-bearing zones in the OIF have a close relationship with quartz veins. The features of gold enrichment at George Lake are inconsistent with syngenetic processes of deposition. Both modified syngenetic and epigenetic processes would produce deposits similar in appearance, since both involve the movement of gold-bearing fluids through the iron formation. In a modified syngenetic deposit, gold originally contained in the iron formation is remobilized by later fluids and deposited adjacent to the fractures through which these fluids travelled. Since the iron formation itself would be the source of the gold, those areas of the iron formation not affected by fluid infiltration would contain significant gold concentrations. However, at George Lake, the OIF away from quartz veins contains negligible gold. Gold-bearing zones typically occur in the OIF as halos, containing gold, pyrrhotite replacing magnetite, arsenopyrite, hornblende replacing grunerite, and chlorite, surrounding quartz veins. This study has shown that the above features are consistent with an epigenetic model for gold deposition.

A well-documented means of epigenetic gold deposition is by the process of sulfidation (Phillips et al. 1984, Hannington and Scott 1989, Lhotka 1988). This process involves the introduction of gold- and sulfur-bearing fluids to an iron-rich host rock, and the subsequent deposition of iron sulfides and

gold. Four sulfidation reactions were presented involving the reaction of either magnetite or iron silicates and the production of either pyrite or pyrrhotite. The observed mineralogy of both unmineralized and mineralized OIF suggests that the two reactions which involve the production of pyrrhotite are most likely to have occurred at George Lake;

$$2\ Fe_3O_4 + 3\ HAu(HS)_2 = 6\ FeS + 9/2\ H_2O + 7/4\ O_2 + 3\ Au \quad \textbf{(7)}$$

$$2\ FeO_{(silicates)} + HAu(HS)_2 = 2\ FeS + 3/2\ H_2O + 1/2\ O_2 + Au \quad \textbf{(8)}$$

The observed replacement of magnetite by pyrrhotite strongly suggests that reaction (7) was significant in the sulfidation process at George Lake. Four iron silicates which may have participated in reaction (8) are present in the OIF. Of these, grunerite was considered the most likely to have undergone sulfidation. Microprobe analyses of grunerites from both unmineralized and mineralized OIF was conducted and X_{Fe} values for each analysis were calculated. Had grunerite participated in reaction (8), a loss of iron would be expected, and grunerites from mineralized OIF would have lower X_{Fe} values than those from unmineralized OIF. Results from this study show that both the range in, and average, X_{Fe} values are similar for both sets of grunerites. No quantifiable loss of iron from grunerites could be established, leading to the conclusion that reaction (8) was not significant in the sulfidation process at George Lake. The primary, if not exclusive, source of iron for sulfidation of the OIF is interpreted to be magnetite.

Interpretation of the results of this study has led to the development of the following model for the genesis of gold deposits at George Lake. Silicate- and oxide iron formation were deposited in the George Lake area around 2683 +/- 1.5 Ma (van Breeman et al. 1992) ago amidst the deposition of Beechy Lake Group turbidites. The area underwent low- to middle-greenschist facies metamorphism, and was subjected to numerous deformational events, including both folding and faulting (Chandler and Holmberg 1990). These fractures acted as conduits for the introduction of hydrothermal fluids to the area. The fluids were rich in gold-bisulfide complexes, arsenic, and calcium. Although the fluids were enriched in sulfur with respect to the OIF, their fO_2 is interpreted to have

been in approximate equilibrium with the OIF. As the fluids passes through the OIF, they deposited hornblende at the edges of grunerite grains, arsenopyrite and chlorite. When sufficient sulfur had been added to the OIF, magnetite began reacting, according to reaction (7), to form pyrrhotite. This caused the destabilization of the gold-bisulfide complexes, and the concomitant deposition of gold. Because the fluid oxygen fugacity was in approximate equilibrium with the unmineralized OIF, and likely with the silicate iron formation as well, grunerites in these units were not affected by the addition of sulfur to the system, and did not participate in the sulfidation process.

Gold deposition at George Lake is interpreted to be a function of several factors; 1) the presence of structural conduits, providing fluid access to the iron formation, and 2) the presence and abundance of magnetite in OIF, forming a favourable horizon for the deposition of gold.

Recommendations

A number of topics for future work, which may contribute to a better understanding of the processes of gold deposition at George Lake, were recognized during the course of this study. The results of thin section analysis and the microprobe analysis of grunerites aided in the interpretation of the specific processes of sulfidation which occurred at George Lake, through the construction and examination of a mineral stability field diagram. This diagram allowed for the indirect determination of the sulfur and oxygen fugacities of both the unmineralized OIF, and the infiltrating mineralizing fluids. However, no direct measurements of these fluids were conducted. A future study based on direct fluid analysis, using fluid inclusions, is recommended in order to determine the temperature of the mineralizing fluids, and their chemical signature. Secondly, samples of silicate iron formation were not obtained for this study. Microprobe analysis of grunerites from this type of iron formation would provide a valuable comparison to the results of the grunerite analyses made in this study, and would aid in a more comprehensive understanding of the sulfidation process at George Lake. Specifically, a study of grunerites from the silicate iron formation

may explain why this unit was not significantly mineralized by the sulfur- and gold-bearing fluids. Lastly, further examination of both unmineralized and mineralized OIF from George Lake may reveal potential methods of excess oxygen fixation. A thorough review of graphite concentrations, sulfate occurrences, and variations in magnetite and grunerite content may help to determine the process by which excess oxygen, produced during the sulfidation of OIF at George Lake, was fixed.

REFERENCES

Ayres, D.E., 1972, Genesis of iron-bearing minerals in banded iron formation mesobands in the Dales Gorge Member, Hamersley Group, Western Australia, Economic Geology, v. 67, p. 1214-1233.

Caddey, S.W., Bachman, R.L., Campbell, T.J., Reid, R.R., and Otto, R.P., 1991, The Homestake gold mine, An early Proterozoic iron-formation-hosted gold deposit, Lawrence County, South Dakota, U.S. Geological Survey Bulletin 1857, Chapter J.

Card, K.D., and King, J.E., 1992, The tectonic evolution of the Superior and Slave provinces of the Canadian Shield: Introduction, Canadian Journal of Earth Sciences, v. 29, p. 2059-2065.

Chandler, T.E., and Holmberg, H.W., 1990, Geology of gold deposits at George Lake area, Back River region, N.W.T.: An Exploration Overview, *in* Proceedings, 4th Western Conference on Precious Metals and the Environment, American Institute of Mining and Metallurgical Engineers, Lead, South Dakota, p. 361-370.

Colvine, A.C., Fyon, J.A., Heather, K.B., Marmont, S., Smith, P.M., and Troop, D.G., 1988, Archean Lode Gold Deposits in Ontario, Ontario Geological Survey, Mines and Minerals Division, Miscellaneous Paper 139, 136 pp.

Deer, W.A., Howie, R.A., and Zussman. J., 1985, An Introduction to the Rock Forming Minerals. 15th edition, Published by Longman Group Ltd., Essex, England, 528 pp.

Floran, R.J., and Papike, J.J., 1978, Mineralogy and petrology of the Gunflint iron-formation, Minnesota-Ontario - Correlation of compositional and assemblage variations at low to moderate grade, Journal of Petrology, v. 19, p. 214-288.

Groves, D.I., Ho, S.E., McNaughton, N.J., Mueller, A.G., Perring, C.S., Rock, N.M.S., and Skwarnecki, M.S., 1988, Genetic models for Archaean lode-gold deposits in Western Australia, *in* Ho, S.E., and Groves, D.I., eds., Advances in Understanding Precambrian Gold Deposits, Volume 2, Geology Department and University Extension, University of Western Australia, Publication No. 12, p. 1-22.

Groves, D.I., Phillips, G.N., Falconer, L.J., Houstoun, S.M., Ho, S.E., Browning, P.,Dahl, N., and McNaughton, N.J., 1987, Evidence for an epigenetic origin for BIF-hosted gold deposits in greenstone belts of the Yilgarn Block, Western Australia, *in* Ho, S.E., and Groves, D.I., eds., Recent Advances in Understanding Precambrian Gold Deposits, Geology Department and University Extension, University of Western Australia, Publication No. 11, p. 167-179.

Fripp, R.E.P., 1976, Stratabound gold deposits in Archean banded iron-formation, Rhodesia, Economic Geology, v. 71, p. 58-75.

Frith, R.A., 1987, Precambrian geology of the Hackett River area, District of Mackenzie, N.W.T., Geological Survey of Canada Memoir 417.

Hannington, M.D., and Scott, S.D., 1989, Sulfidation Equilibria as guides to gold mineralization in volcanogenic massive sulfides: Evidence from sulfide mineralogy and the composition of sphalerite, Economic Geology, v. 84, p. 1978-1995.

Hasse, C.S., 1982, Metamorphic petrology of the Negaunee iron formation, Marquette District, northern Michigan: Mineralogy, metamorphic reactions and phase equilibria, Economic Geology, v. 77, p. 60-81.

Hoffman, P.F., 1989, Precambrian geology and tectonic history of North America, *in* Bally, A.W., and Palmer, A.R., eds., The Geology of North America - An overview, Geological Society of America, The Geology of North America, v. A, p. 447-512.

Holland, T.J.B., and Powell, R., 1990, An enlarged and updated internally consistent thermodynamic data set with uncertainties and correlations: the system K_2O-Na_2O-CaO-MgO-FeO-Fe_2O_3-Al_2O_3-TiO_2-SiO_2-C-H_2-O_2, Journal of Metamorphic Geology, v. 8, p. 89-124.

Jefferson, C.W., Beaumont-Smith, C.J., and Lustwerk, R., 1989, Stratigraphic and structural settings of iron formation and gold in the Back River area, District of Mackenzie, N.W.T., *in* Current Research, Part C, Geological Survey of Canada Paper 89-1C, p. 293-304.

Jefferson, C.W., Lustwerk, R., and Lambert, M.B., 1992, Stratigraphy, facies changes and structure in auriferous iron-rich Archean sedimentary sequences around the Back River Volcanic Complex, northeastern Slave province, N.W.T, Geological Survey of Canada Open File 2484, p. 185-188.

Jefferson, C.W., Lustwerk, R., Lambert, M.B., Fumerton, S., Hudson, K., and Olson, R.A., 1989, Structure, stratigraphy and changes in auriferous iron-rich Archean sedimentary rocks of northeastern Slave province, N.W.T., *in* Exploration Overview 1989, Northwest Territories: Mining, Exploration and Geological Investigations, p. 42.

Kerswill, J.A., 1984, The Lupin gold deposit, Contwoyto Lake area, N.W.T.; Styles of gold distribution and possible genetic models, Geological Association of Canada Program with Abstracts, v. 9, p. 78.

Kerswill, J.A., 1986, Gold deposits hosted by iron formation in the Contwoyto Lake area, Northwest Territories, *in* Chater, A.M., ed., Gold '86 Poster Paper Abstracts, Geological Association of Canada, Mineral Deposits Division, p. 82-85.

Kerswill, J.A., 1992, Gold metallogeny of the Contwoyto Lake, Russell Lake and Courageous lake areas, Slave Province, N.W.T., Geological Survey of Canada Open File 2484, p. 161-167.

Klein, C., 1973, Changes i mineral assemblages with metamorphism of some banded Precambrian iron-formations, Economic Geology, v. 68, p. 1075-1088.

Lambert, M.B., 1976, The Back River Volcanic Complex, District of Mackenzie, *in* Report on Activities, Part A, Geological Survey of Canada Paper 76-1A, p. 363-367.

Lambert, M.B., Burbidge, G., Jefferson, C.W., Beaumont-Smith, C., and Lustwerk, R., 1990, Stratigraphy, facies and structure in volcanic and sedimentary rocks of the Archean Back River Volcanic Complex, N.W.T., *in* Current Research, Part C, Geological Survey of Canada Paper 90-1C, p. 151-165.

Lhotka, P.G., 1988, Geology and geochemistry of gold-bearing iron formation in the Contwoyto Lake - Point Lake region, Northwest Territories, Canada, Unpublished Ph.D. Thesis, University of Alberta, Edmonton, Alberta.

Lhotka, P.G., and Nesbitt, B.E., 1989, Geology of unmineralized and gold-bearing iron formation, Contwoyto Lake - Point Lake region, Northwest Territories, Canada, Canadian Journal of Earth Sciences, v. 26, p. 46-64.

Macdonald, A.J., and Fyon, J.A., 1986, Sulfidation - The key to Gold Mineralization in banded iron formation, *in* Chater, A.M., ed., Gold '86 Poster Paper Abstracts, Geological Association of Canada, Mineral Deposits Division, p. 96-97.

McGlynn, J.C., and Henderson, J.B., 1972, The Slave Province, *in* Price, R.A., and Douglas J.W., eds., Variations in Tectonic Styles in Canada, Geological Association of Canada, Special Paper 11, p. 505-526.

McGlynn, J.C., 1977, Geology of Bear-Slave Structural provinces, District of Mackenzie, Geological Survey of Canada Open File 445.

Padgham, W.A., 1992, Mineral deposits in the Archean Slave Structural province; lithological and tectonic setting, Precambrian Research, v. 58, p. 1-24.

Padgham, W.A., and Fyson, W.K., 1992, The Slave Province: a distinct Archean craton, Canadian Journal of Earth Sciences, v. 29, p. 2072-2086.

Phillips, G.N., Groves, D.I., and Martyn, J.E., 1984, An epigenetic origin for Archean banded iron-formation-hosted gold deposits, Economic Geology, v. 79, p. 162-171.

Robie, R.A., Hemingway, B.S., and Fisher, J.R., 1979, Thermodynamic properties of minerals and related substances at 298.15 K and 1 Bar (10^5 Pascals) pressure and at higher temperatures, U.S. Geological Survey Bulletin 1452, 456 pp.

Rye, D.M., and Rye, R.O., 1974, Homestake gold mine, South Dakota: I. Stable isotope studies, Economic Geology, v. 69, p. 293-317.

Saager, R., Oberthur, T., and Tomschi, H.P., 1987, Geochemistry and mineralogy of banded iron formation-hosted gold mineralization in the Gwanda greenstone belt, Zimbabwe, Economic Geology, v. 82, p. 2017, 2032.

Seward, T.M., 1984, The transport and deposition of gold in hydrothermal systems, *in* Foster, R.P., ed., Gold'82: The geology, geochemistry and genesis of gold deposits, Geological Society of Zimbabwe Special Publication No. 1, p. 165-181.

Tremblay, L.P., 1971, Geology of Beechy Lake map-area, District of Mackenzie, Geological Survey of Canada Memoir 365.

van Breeman, O., Jefferson, C.W., and Bursey, T., 1992, Precise 2683 Ma age of turbidite-hosted auriferous iron formations in the vicinity of George Lake, eastern Slave Structural province, N.W.T., Geological Survey of Canada Open File 2484, p. 205-207.

APPENDIX 1

MINERAL INVENTORY

SAMPLE	TYPE	QTZ	QV	CARG	CARV	GRU	HBL	STP	CHL	BT	ZRN	AP	GR	MAG	PO	APY	PY	CC	ILM	Au
BH1001-1	MIN	X		X				X	X				O	TR	X	O	X		TR	
BH1001-2	MIN	X	O	X				X	X							X	X			TR
BH1001-3	MIN	O	X	X	O									TR	O	X	O			
BH1002	UM	X		X		X		X	O				O	X	O					
BH1003	MIN	X	X	X	O	X			O	TR				TR	X	O				TR
BH1004A	UM		X		O	X	O	X	X						O			TR		
BH1004B-1	UM		X	X	O	X		X	X	O			O	O	O					
BH1004B-2	UM	X	O	X		X		O	O	O			O	TR	TR					
BH1006	MIN	X		X		X			X	O				TR	X					
BH1007	UM	X		X		X		O	X					X	X			TR		
BH1008A	MIN		X		O	X		O	X					TR	O	O				
BH1008B-1	MIN	O	X	X		X		O	X						X			TR		
BH1008B-2	MIN	X	O	O		X		O	X	TR				TR	X				TR	
BH1009A	MIN	O	X	X	X			O	X	O					O	O		O	O	TR
BH1011	UM	X		X	X	X		X	O					X	O					
BH1012	UM	X		TR		X	TR		X	O	O			O	O					
BH1013B	MIN		X			X	X	X	X					O	O					
BH1014	UM	O				X	X		X	X	TR		O	TR						
BH1015	UM	X		O		X	O	O						O	O					
BH1016	UM	X				X	TR	X	O					X	O					
BH1017	UM	X				X		O	X	TR			X	X	O					
BH1018	MIN	X	X			X		O	X	O			O	X	X	TR	TR			
BH1019-1	MIN	O	X	O	X	X		O	X	X				O	O					
BH1019-2	MIN		X		O				X	O				O	O					
BH1020	UM	X		O		X		O	X	TR			O	X	O					
BH1021	UM	X		X		X	TR	O	X				TR	TR	O			TR		
BH1022	MIN	X	X			X	O	O	O					O	TR					
BH1023	UM	X		X		X		X						X	O					
BH1024	MIN	O		X		X			X					O	X	X				TR
BH1026	MIN	X		X				TR	X						X			TR		
BH1032	UM	X		O	O	X			O				O	X	O					
BH1034A	MIN		X		O			X	O						O	O		TR		
BH1037	UM	X	O	X	O	X		O	X	O				X	O					
BH1040	UM	X		X		X			X	TR				TR	TR					
BH1041A	MIN	X	O	X		X		X	X					X	X					
BH1041B	MIN	X		X		X		O	X					O	X			TR		
BH1043	UM	X		X				X	X					X	O					

SAMPLE	TYPE	QTZ	QV	CARG	CARV	GRU	HBL	STP	CHL	BT	ZRN	AP	GR	MAG	PO	APY	PY	CC	ILM	Au
BH1045A	UM	X	O	X	O			O	X				O	TR	TR					
BH1045B-1	MIN	X	X	X	X			O	O				TR	TR	O	O	O	TR		
BH1046A	MIN	X	O	O		X		O	O	O	TR				O	TR		TR		
BH1046B	MIN	O	X	X	O	O		O	O					TR	X		O	TR		
BH1046C	MIN	X	O	X		X		O	X	O				TR	O	X				TR
BH1047	UM	X		X	O	X		O	O				O	X	TR					
BH1050A	MIN		X		X	O	O	O	X				O	TR	O	X				TR
BH1050B	MIN	X	X	X	X	O	O	O	O	X	O				O	X				TR
BH1050C-1	UM	X		X		X		O	X				X		O	TR			TR	
BH1050C-2	UM	X				X	O	X	O	O				TR	O			TR		
BH1053A	MIN	X	O	X		X		O	O					TR	X				TR	
BH1053B	MIN	X		X		X			X				O	TR	X	O		TR		
BH1055A	MIN		O		TR			TR	X	O	TR		TR		O	O			TR	TR
BH1055B-1	MIN	X		O		X		O	X						X		TR			TR
BH1055B-2	MIN	X		X		X		X	O					TR	X		TR			
BH1055B-3	MIN	X		X		X		TR	O						X		TR			
BH1056	MIN	X		O		X	X	O	O					TR	X	X	O	TR		
BH1057	MIN	X	X		O			O	O	TR					O	O		TR		
BH1059	UM	X				X	O	O			TR			X	TR					
BH1060	UM	X	O	X		X		O	X	X	TR			TR	TR					
BH1062	MIN	TR	TR	X	X			O	X						O	O	O		TR	
BH1063A-2	MIN	X	X	X	X	X		X	X					O	O	X		TR		
BH1063B	MIN	X		X				X	O					TR	X	TR	O			
BH1066A	MIN	X	O	X	O			O	X					TR	TR		X		TR	
BH1066B	MIN	X	X	X	X			X	X						TR		X			
BH1073A	UM	X		TR		X		O	O	O	TR			O	TR					
BH1073B	UM	O		O	TR	X			X	X	TR				TR					
BH1074	UM	X		X		X		TR	O					X	O					
BH1076	MIN	X	X	X	X	X		O	X	O				O	X	X		TR	TR	TR
BH1078A	MIN	X	O			X	O	O	X	X			X	TR	X	TR				
BH1078B	MIN	X	X	X	O	X	X	O	O	O				O	X		TR	TR		
BH1080A-1	MIN	X	O	X	O	X		O	O					O	X					
BH1080A-2	MIN	X	X	X	O	X		X	O						X	O		TR		
BH1080A-3	MIN	X	X	X	X	X		O	O					TR	X	O		TR		
BH1080B	MIN	X	X	X	X	X		O	O						O	X		TR		
BH1080C	MIN		X		X	O		O								O				
BH1081	UM	X		X		X		O	O				O	X	O					

SAMPLE	TYPE	QTZ	QV	CARG	CARV	GRU	HBL	STP	CHL	BT	ZRN	AP	GR	MAG	PO	APY	PY	CC	ILM	Au
BH2001A	UM	X				X	X	X		O				O	O		TR			
BH2001B	UM	X		O		X	X	X		O	TR			O	O					
BH2005A-1	MIN	X				X	X	O	O	O	TR				X	X	TR		TR	TR
BH2005A-2	MIN	O	X	O		X	X	X	X	O				TR	X	O				
BH2005B-1	MIN	X	O			X	X	O	X	TR				TR	X	O		TR		TR
BH2005B-2	MIN	X	X			X	X	X	X	O				TR	X	O		O	TR	
BH2005C	MIN	O	X		X	X	X	O	X			TR		TR	TR					
BH2006	MIN	X				X	O	O	X						X	X		O		TR
BH2007	UM					X	X	X	X	O			X	TR	TR			TR		
BH2010	MIN	O				X	X	X					O		X				TR	
BH2015	MIN	X	X	O		X	X	X					O	O	X					
BH2017	UM	O	X	TR		X		X	X					TR	TR	TR				
BH2018	UM	X	X	X	O	X	O	O	TR				O	O	O					
BH2019	UM	X				X	X			X	TR			X	O			TR		
BH2021	UM	X	X	X		X	O	X						X	O					
BH2024	UM	X				X	O	O	X	O	TR			X	O					
BH2029	UM	X		O		X	O	O		O	TR									
BH2030A	MIN			O	X	X	O	O	X	X	TR			TR	X	O	TR			
BH2030B-1	MIN	O		X		X	O	X	X	O	O			TR	X	O	TR			
BH2030B-2	MIN	X	X			X	X	X	X					TR	X				TR	
BH2031A	MIN		X	O	X	X	O	X	X					TR	TR	X				
BH2031B	MIN			X	X	X		O						TR	TR	X				
BH2031C	MIN			X		X	O	O	X	O	TR				X	O				
BH2033	UM	X	X	TR		X	X	X		O				TR	TR					
BH2036A	MIN	X	X		O	X	O	O	X					TR	X		TR			
BH2036B	MIN	X			O	X	O	X	TR	O				X	X	O	TR			
BH2040	UM	X	O			X	O	O					O	TR	TR					
BH2046	MIN	O	X	TR		X	O	O	O				O		X		TR			
BH2047	UM					X	X	X	O						TR					
BH2048-1	MIN	X	X	X	O	O		O				O			X	TR		TR		
BH2048-2	MIN	X	O	O		X		X	O	O				O	X	TR				
BH2049	MIN	X	X	O				X	X						O	O				
BH2051-1	MIN		O		X	O		X	O					TR	TR					
BH2051-2	MIN	O	X		O	X	X	X	X					O	O	O				
BH2053	UM	O	X	O		X	X	X						TR	TR					
BH2054	MIN	X		X		X	O	X	O					O	X			TR		
BH2056	UM	X	O			X	O	X	X											

SAMPLE	TYPE	QTZ	QV	CARG	CARV	GRU	HBL	STP	CHL	BT	ZRN	AP	GR	MAG	PO	APY	PY	CC	ILM	Au
BH2058	MIN	X	X	O				X	O								X		TR	
BH2061	MIN	X	X	X	O			X	X						TR	X				
BH2064	UM	X		X		X	O	X					O	X	O					
BH2066	MIN	X		O		X	O	O						X	O					
BH2070	UM	X				X		X	O					O	TR					
BH2072A	UM	X	O			X	O	O	O					X	O					
BH2072B	UM		O	O	O	X			X	X	TR									
BH2072C	UM	O	X	O		X	O	X	X	O	TR			TR						
BH2075A	UM	X		X		X	O	X	X				TR		TR					
BH2075B	UM	X	O	O		X	O	O	O					X	O					
BH2077	MIN	X				X	O	O	O						O	O				
BH2085	MIN	X	X	X	X	X	O	X	O					TR	X					
BH2100	MIN	O	X	X	X			X	O							TR	X		TR	TR
BH2105A	MIN	X		O		O		X	O						X		X			
BH2105B	MIN	X				O		X	X	O					X		X	O		
BH2105C	MIN	X	X	O	O	X		X	X					TR	O	TR	O			

EXPLANATION:

MIN= Mineralized Oxide Iron Formation
UM= Unmineralized Oxide Iron Formation
X= Mineral Present and >/= 5%
O= Mineral Present and = 0.5–5%
TR= Mineral Present and </= 0.5%
BLANK= Mineral Not Present

QTZ= Quartz in groundmass
QV= Vein quartz
CARG= Carbonate in groundmass
CARV= Vein Carbonate
GRU= Grunerite
HBL= Hornblende

STP= Stipnomelane
CHL= Chlorite
BT= Biotite
ZRN= Zircon
AP= Apatite
GR= Graphite

MAG= Magnetite
PO= Pyrrhotite
APY= Arsenopyrite
CC= Chalcopyrite
ILM= Ilmenite
Au= Visible Gold

APPENDIX 2

MICROPROBE ANALYSES

Sample	BH2047	BH2047	BH2047	BH2047	BH2047	BH2047	BH2047	BH2047	BH2047	BH2047	BH2047	BH2047
Type	UM	UM	UM	UM	UM	UM	UM	UM	UM	UM	UM	UM
Mineral	GRU	GRU	GRU	GRU	GRU	GRU	GRU	GRU	GRU	GRU	GRU	GRU
SiO2	51.02	49.91	50.83	51.45	50.73	51.11	50.97	50.58	50.46	50.29	50.55	50.73
TiO2	0.00	0.00	0.03	0.00	0.01	0.03	0.01	0.01	0.02	0.01	0.03	0.00
Al2O3	0.36	0.82	0.28	0.26	0.29	0.24	0.27	0.17	0.25	0.22	0.30	0.47
FeO	38.79	38.55	40.25	39.09	40.83	39.84	40.42	40.57	39.96	40.40	39.68	40.70
MnO	0.04	0.01	0.04	0.02	0.04	0.04	0.02	0.06	0.03	0.02	0.03	0.03
MgO	8.40	7.05	7.31	7.83	6.73	6.89	7.01	6.93	6.92	6.55	7.29	6.53
CaO	0.29	1.42	0.45	0.35	0.44	0.41	0.46	0.46	0.37	0.48	0.35	0.54
Na2O	0.11	0.10	0.05	0.12	0.03	0.00	0.07	0.03	0.08	0.07	0.06	0.09
K2O	0.00	0.09	0.00	0.00	0.00	0.00	0.00	0.00	0.00	0.00	0.00	0.00
Total	99.01	97.95	99.23	99.11	99.11	98.55	99.23	98.81	98.10	98.34	98.28	99.09
Cations based on 23 O												
Si	7.9242	7.8782	7.9364	7.9834	7.9532	8.0108	7.9608	7.9515	7.9692	7.9452	7.9536	7.9503
Ti	0.0000	0.0000	0.0030	0.0000	0.0012	0.0032	0.0013	0.0018	0.0023	0.0016	0.0037	0.0000
Al	0.0653	0.1528	0.0508	0.0478	0.0537	0.0442	0.0490	0.0307	0.0467	0.0403	0.0549	0.0873
Fe	5.0383	5.0880	5.2556	5.0717	5.3529	5.2212	5.2795	5.3327	5.2773	5.3376	5.2207	5.3339
Mn	0.0054	0.0016	0.0059	0.0030	0.0053	0.0058	0.0026	0.0084	0.0036	0.0033	0.0037	0.0035
Mg	1.9441	1.6587	1.7007	1.8108	1.5729	1.6097	1.6312	1.6236	1.6293	1.6133	1.7096	1.5256
Ca	0.0486	0.2407	0.0748	0.0576	0.0744	0.0681	0.0771	0.0776	0.0632	0.0806	0.0586	0.0912
Na	0.0326	0.0310	0.0140	0.0347	0.0082	0.0000	0.0221	0.0082	0.0253	0.0209	0.0185	0.0267
K	0.0000	0.0179	0.0000	0.0000	0.0000	0.0000	0.0000	0.0000	0.0000	0.0000	0.0000	0.0000
Sum	15.0585	15.0688	15.0412	15.0090	15.0218	14.9630	15.0236	15.0345	15.0169	15.0428	15.0233	15.0185
Fe/(Fe+Mg)	0.7216	0.7541	0.7555	0.7369	0.7729	0.7644	0.7640	0.7666	0.7641	0.7679	0.7533	0.7776

UM = unmineralized, MIN = mineralized, GRU = grunerite, HBL = hornblende, BI = biotite, STP = stipnomelane

Sample	BH2047	BH2047	BH2047	BH2047	BH2047	BH2047	BH2024	BH2024	BH2036B	BH2036B	BH2036B	BH2036B
Type	UM	UM	UM	UM	UM	UM	UM	UM	MIN	MIN	MIN	MIN
Mineral	HBL	HBL	HBL	HBL	HBL	HBL	BI	BI	GRU	GRU	HBL	BI
SiO2	40.85	41.47	39.85	41.61	41.33	41.33	29.43	30.39	49.61	49.70	39.97	42.77
TiO2	0.07	0.08	0.07	0.14	0.09	0.09	0.74	0.81	0.00	0.01	0.20	0.00
Al2O3	14.11	13.91	13.90	9.68	13.35	14.34	18.08	18.18	0.31	0.37	14.79	6.38
FeO	27.24	27.93	29.22	29.42	27.50	27.17	32.49	29.93	42.29	42.15	27.82	32.24
MnO	0.02	0.00	0.00	0.00	0.00	0.02	0.04	0.07	0.17	0.10	0.02	0.04
MgO	2.99	3.11	3.49	4.57	3.15	3.09	6.44	5.97	5.12	5.51	2.10	2.76
CaO	11.16	11.12	9.92	10.27	11.14	11.31	0.00	0.02	0.33	0.30	11.09	0.00
Na2O	1.35	1.40	1.20	0.93	1.38	1.33	0.06	0.05	0.03	0.11	1.31	0.61
K2O	0.42	0.38	0.37	0.30	0.38	0.37	4.69	6.15	0.00	0.00	0.51	5.89
Total	98.21	99.41	98.03	96.92	98.33	99.05	91.97	91.57	97.88	98.26	97.79	90.68
Cations based on 23 O												
Si	6.3681	6.3944	6.2749	6.6433	6.4389	6.3736	5.1360	5.2898	7.9622	7.9348	6.2852	7.4366
Ti	0.0081	0.0091	0.0088	0.0170	0.0100	0.0107	0.0973	0.1064	0.0000	0.0012	0.0241	0.0000
Al	2.5919	2.5279	2.5800	1.8221	2.4521	2.6064	3.7190	3.7299	0.0591	0.0702	2.7411	1.3069
Fe	3.5502	3.6005	3.8477	3.9281	3.5822	3.5043	4.7411	4.3570	5.6755	5.6271	3.6576	4.6876
Mn	0.0028	0.0000	0.0000	0.0000	0.0000	0.0028	0.0061	0.0107	0.0225	0.0134	0.0020	0.0062
Mg	0.6956	0.7149	0.8195	1.0869	0.7322	0.7107	1.6745	1.5490	1.2257	1.3117	0.4915	0.7152
Ca	1.8644	1.8375	1.6731	1.7565	1.8601	1.8683	0.0000	0.0046	0.0574	0.0521	1.8676	0.0000
Na	0.4088	0.4199	0.3676	0.2870	0.4176	0.3966	0.0205	0.0155	0.0098	0.0347	0.3985	0.2067
K	0.0826	0.0749	0.0753	0.0605	0.0759	0.0726	1.0440	1.3650	0.0000	0.0000	0.1017	1.3059
Sum	15.5725	15.5791	15.6469	15.6014	15.5690	15.5460	16.4385	16.4279	15.0122	15.0452	15.5693	15.6651
Fe/(Fe+Mg)	0.8362	0.8343	0.8244	0.7833	0.8303	0.8314	0.7390	0.7377	0.8224	0.8110	0.8815	0.8676

Sample	BH2061	BH2061	BH2061	BH2061	BH2030B-2	BH2030B-2	BH2030B-2	BH2030B-2	BH2030B-2	BH2033	BH2033	BH2033
Type	MIN	MIN	MIN	MIN	MIN	MIN	MIN	MIN	MIN	UM	UM	UM
Mineral	STP	STP	STP	STP	GRU	GRU	GRU	HBL	HBL	GRU	GRU	GRU
SiO2	46.08	46.17	46.90	45.08	48.73	48.63	50.04	39.64	39.62	49.78	49.85	49.38
TiO2	0.01	0.03	0.01	0.00	0.02	0.00	0.00	0.23	0.21	0.04	0.00	0.00
Al2O3	5.38	5.40	5.46	5.26	0.24	0.19	0.18	14.56	14.57	0.32	0.41	0.41
FeO	34.31	34.29	34.74	34.63	43.09	42.51	43.38	29.45	29.14	41.06	39.49	40.97
MnO	0.08	0.13	0.10	0.08	0.24	0.26	0.30	0.16	0.07	0.11	0.06	0.08
MgO	2.75	2.80	2.63	2.82	4.67	4.72	5.01	1.86	1.89	5.29	6.01	4.86
CaO	0.04	0.03	0.02	0.01	0.27	0.37	0.31	11.12	10.87	0.40	0.33	0.45
Na2O	0.14	0.23	0.16	0.24	0.10	0.05	0.00	1.32	1.59	0.06	0.00	0.09
K2O	1.62	1.74	1.96	2.16	0.00	0.00	0.00	0.50	0.50	0.00	0.00	0.00
Total	90.41	90.83	91.97	90.29	97.36	96.73	99.22	98.84	98.47	97.05	96.15	96.23
Cations based on 23 O												
Si	7.8068	7.7929	7.8199	7.7191	7.9200	7.9413	7.9515	6.2265	6.2378	8.0081	8.0285	8.0197
Ti	0.0014	0.0038	0.0013	0.0000	0.0027	0.0000	0.0000	0.0270	0.0251	0.0044	0.0000	0.0000
Al	1.0733	1.0747	1.0721	1.0622	0.0459	0.0368	0.0342	2.6951	2.7042	0.0598	0.0774	0.0788
Fe	4.8611	4.8399	4.8436	4.9586	5.8566	5.8038	5.7642	3.8685	3.8370	5.5224	5.3180	5.5629
Mn	0.0109	0.0190	0.0141	0.0121	0.0328	0.0036	0.0400	0.0207	0.0099	0.0146	0.0087	0.0106
Mg	0.6950	0.7043	0.6533	0.7196	1.1319	1.1482	1.1873	0.4367	0.4436	1.2685	1.4429	1.1758
Ca	0.0079	0.0056	0.0032	0.0026	0.0473	0.0648	0.0532	1.8722	1.8341	0.0697	0.0563	0.0788
Na	0.0444	0.0753	0.0520	0.0782	0.0328	0.0156	0.0000	0.4032	0.4846	0.0183	0.0000	0.0269
K	0.3509	0.3740	0.4162	0.4709	0.0000	0.0000	0.0000	0.0997	0.0997	0.0000	0.0000	0.0000
Sum	14.8517	14.8895	14.8757	15.0233	15.0696	15.0141	15.0304	15.6496	15.6760	14.9658	14.9318	14.9535
Fe/(Fe+Mg)	0.8749	0.8730	0.8812	0.8733	0.8380	0.8348	0.8292	0.8986	0.8964	0.8132	0.7866	0.8255

Sample	BH2033	BH2033	BH2033	BH2033	BH2033	BH2033	BH2033	BH2033	BH2033	BH2033	BH2033	BH2033
Type	UM	UM	UM	UM	UM	UM	UM	UM	UM	UM	UM	UM
Mineral	GRU	GRU	GRU	GRU	GRU	GRU	HBL	HBL	HBL	HBL	HBL	HBL
SiO2	50.05	48.74	49.57	49.16	49.24	49.98	39.85	40.84	40.35	39.88	39.84	40.47
TiO2	0.02	0.00	0.00	0.00	0.01	0.00	0.16	0.15	0.18	0.23	0.10	0.15
Al2O3	0.35	1.59	0.65	1.33	0.49	0.43	13.81	12.86	12.58	13.91	14.75	13.19
FeO	41.71	40.29	41.23	40.65	40.53	40.81	27.79	22.22	28.19	27.74	27.77	27.87
MnO	0.07	0.05	0.06	0.03	0.07	0.00	0.00	0.01	0.00	0.07	0.00	0.05
MgO	4.82	4.54	4.66	4.58	5.38	5.40	1.95	2.14	2.21	1.92	1.82	2.16
CaO	0.40	1.43	0.62	1.20	0.46	0.47	12.46	12.39	11.71	12.28	12.27	12.38
Na2O	0.02	0.11	0.10	0.20	0.05	0.05	1.25	1.20	0.99	1.24	1.27	1.33
K2O	0.00	0.00	0.00	0.00	0.00	0.07	0.46	0.41	0.39	0.43	0.48	0.44
Total	97.43	96.75	96.88	97.15	96.23	97.22	97.75	98.21	96.62	97.70	98.29	98.03
Cations based on 23 O												
Si	8.0326	7.8703	7.9988	7.9070	7.9819	8.0104	6.3047	6.4285	6.4519	6.3057	6.2536	6.3804
Ti	0.0020	0.0000	0.0000	0.0000	0.0018	0.0000	0.0192	0.0174	0.0220	0.0278	0.0019	0.0172
Al	0.0661	0.3030	0.1241	0.2522	0.0940	0.0816	2.5755	2.3847	2.3704	2.5914	2.7292	2.4504
Fe	5.5971	5.4405	5.5630	5.4673	5.4944	5.4686	3.6767	3.7142	3.7684	3.6687	3.6452	3.6741
Mn	0.0094	0.0068	0.0077	0.0038	0.0092	0.0000	0.0000	0.0016	0.0000	0.0088	0.0000	0.0071
Mg	1.1528	1.0930	1.1219	1.0989	1.2997	1.2911	0.4606	0.5018	0.5273	0.4536	0.4253	0.5076
Ca	0.0683	0.2466	0.1071	0.2060	0.0793	0.0810	2.1120	2.0887	2.0057	2.0805	2.0629	2.0908
Na	0.0061	0.0342	0.0314	0.0616	0.0160	0.0151	0.3849	0.3659	0.3078	0.3809	0.3853	0.4076
K	0.0000	0.0000	0.0000	0.0000	0.0000	0.0015	0.0926	0.0822	0.0805	0.0859	0.0964	0.0894
Sum	14.9344	14.9944	14.9540	14.9968	14.9763	14.9493	15.6262	15.5850	15.5340	15.6033	15.5998	15.6246
Fe/(Fe+Mg)	0.8292	0.8327	0.8322	0.8326	0.8087	0.8090	0.8887	0.8810	0.8772	0.8900	0.8955	0.8786

Sample	BH2033	BH2033	BH2033	BH2033	BH2033	BH2030B-2	BH2030B-2	BH2030B-2	BH2030B-2	BH2030B-2	BH2030B-2	BH2029
Type	UM	UM	UM	UM	UM	MIN	MIN	MIN	MIN	MIN	MIN	UM
Mineral	HBL	HBL	HBL	HBL	HBL	GRU	GRU	GRU	GRU	HBL	HBL	GRU
SiO2	40.28	40.23	40.05	40.31	40.27	49.71	49.55	49.81	48.92	38.96	39.89	49.68
TiO2	0.12	0.18	0.17	0.09	0.09	0.05	0.00	0.00	0.01	0.26	0.21	0.00
Al2O3	13.04	13.23	13.35	13.26	13.35	0.02	0.18	0.20	0.20	13.61	13.34	0.19
FeO	28.20	28.27	28.54	27.71	27.64	43.12	42.51	42.66	43.15	29.36	28.87	42.55
MnO	0.02	0.05	0.00	0.01	0.02	0.21	0.25	0.23	0.27	0.07	0.08	0.00
MgO	2.01	2.24	2.03	2.12	2.05	4.94	4.74	5.03	4.63	2.06	2.04	4.95
CaO	12.11	12.31	12.35	12.20	12.26	0.39	0.43	0.34	0.33	11.58	12.01	0.36
Na2O	1.25	1.42	1.31	1.21	1.34	0.00	0.02	0.00	0.09	1.60	1.59	0.08
K2O	0.42	0.42	0.44	0.44	0.41	0.00	0.00	0.00	0.00	0.48	0.44	0.00
Total	97.45	98.35	98.25	97.37	97.44	98.61	97.68	98.29	97.61	97.99	98.48	97.81
Cations based on 23 O												
Si	6.3963	6.3385	6.3242	6.3908	6.3802	7.9470	7.9846	7.9723	7.9307	6.2094	6.2998	7.9829
Ti	0.0144	0.0210	0.0207	0.0109	0.0112	0.0056	0.0000	0.0000	0.0013	0.0308	0.0253	0.0000
Al	2.4396	2.4566	2.4847	2.4769	2.4931	0.0381	0.0351	0.0377	0.0391	2.5561	2.4827	0.0360
Fe	3.7411	3.7245	3.7694	3.6733	3.6618	5.7646	5.7280	5.7094	5.8491	3.9128	3.8125	5.7182
Mn	0.0021	0.0065	0.0000	0.0019	0.0028	0.0284	0.0347	0.0313	0.0366	0.0096	0.0112	0.0000
Mg	0.4769	0.5267	0.4786	0.5011	0.4842	1.1768	1.1377	1.1994	1.1186	0.4890	0.4799	1.1861
Ca	2.0609	2.0783	2.0896	2.0727	2.0811	0.0669	0.0736	0.0577	0.0580	1.9771	2.0328	0.0626
Na	0.3837	0.4335	0.4019	0.3730	0.4102	0.0000	0.0062	0.0000	0.0280	0.4952	0.4877	0.0247
K	0.0846	0.0850	0.0876	0.0898	0.0829	0.0000	0.0000	0.0000	0.0000	0.0971	0.0892	0.0000
Sum	15.5996	15.6706	15.6567	15.5904	15.6075	15.0274	14.9999	15.0078	15.0614	15.7771	15.7211	15.0105
Fe/(Fe+Mg)	0.8869	0.8761	0.8873	0.8800	0.8832	0.8305	0.8343	0.8264	0.8395	0.8889	0.8882	0.8282

Sample	BH2029	BH2029	BH2029	BH2029	BH2029	BH2029	BH2030B-1	BH2030B-1	BH2030B-1	BH2030B-1	BH2030B-1	BH2030B-1
Type	UM	UM	UM	UM	UM	UM	MIN	MIN	MIN	MIN	MIN	MIN
Mineral	GRU	GRU	GRU	HB	HB	HB	GRU	GRU	GRU	GRU	GRU	GRU
SiO2	50.35	49.39	49.59	39.44	40.53	41.15	49.83	49.72	49.77	49.38	50.31	50.26
TiO2	0.00	0.02	0.00	0.16	0.16	0.09	0.00	0.02	0.00	0.01	0.00	0.01
Al2O3	0.20	0.19	0.17	14.11	14.26	13.93	0.42	0.36	0.31	0.24	0.31	0.16
FeO	42.83	41.38	41.61	28.36	28.20	27.74	41.73	41.32	41.77	41.93	42.30	42.50
MnO	0.03	0.04	0.08	0.07	0.02	0.07	0.25	0.22	0.24	0.19	0.24	0.13
MgO	4.96	6.15	5.79	2.06	2.12	2.21	4.88	5.10	5.02	4.84	4.95	4.97
CaO	0.40	0.29	0.26	12.52	12.44	12.53	0.47	0.38	0.44	0.47	0.29	0.40
Na2O	0.00	0.02	0.03	1.44	1.39	1.16	0.06	0.07	0.13	0.00	0.06	0.01
K2O	0.00	0.00	0.00	0.53	0.47	0.46	0.00	0.00	0.00	0.00	0.00	0.00
Total	98.78	97.47	97.54	98.68	99.59	99.33	97.64	97.19	97.70	97.06	98.45	98.53
Cations based on 23 O												
Si	8.0015	7.9285	7.9600	6.2119	6.2888	6.3753	7.9941	8.0013	7.9872	7.9894	8.0084	8.0045
Ti	0.0000	0.0019	0.0000	0.0184	0.0185	0.0101	0.0000	0.0025	0.0000	0.0016	0.0000	0.0016
Al	0.0380	0.0363	0.0326	2.6181	2.6067	2.5436	0.0789	0.0683	0.0588	0.0454	0.0585	0.0292
Fe	5.6919	5.5543	5.5846	3.7341	3.6580	3.5934	5.5995	5.5595	5.6053	5.6737	5.6304	5.6608
Mn	0.0045	0.0049	0.0104	0.0087	0.0025	0.0088	0.0346	0.0298	0.0332	0.0265	0.0319	0.0182
Mg	1.1741	1.4715	1.3843	0.4835	0.4906	0.5105	1.1681	1.2243	1.2017	1.1674	1.1737	1.1813
Ca	0.0686	0.0501	0.0456	2.1121	2.0671	2.0797	0.0808	0.0650	0.0764	0.0813	0.0496	0.0676
Na	0.0000	0.0061	0.0104	0.4384	0.4191	0.3492	0.0191	0.0208	0.0400	0.0000	0.0181	0.0303
K	0.0000	0.0000	0.0000	0.1073	0.0931	0.0915	0.0000	0.0000	0.0000	0.0000	0.0000	0.0000
Sum	14.9786	15.0536	15.0279	15.7325	15.6444	15.5621	14.9751	14.9715	15.0026	14.9853	14.9706	14.9935
Fe/(Fe+Mg)	0.8290	0.7906	0.8014	0.8854	0.8817	0.8756	0.8274	0.8195	0.8235	0.8294	0.8275	0.8273

Sample	BH2030B-1	BH2030B-1	BH2030B-1	BH2030B-1	BH2030B-1	BH2030B-1	BH2030B-2	BH2030B-2	BH2030B-2	BH2030A	BH2030A	BH2030A
Type	MIN	MIN	MIN	MIN	MIN	MIN	MIN	MIN	MIN	MIN	MIN	MIN
Mineral	GRU	GRU	GRU	GRU	GRU	HBL	HBL	HBL	HBL	GRU	GRU	GRU
SiO2	50.25	50.08	49.45	49.38	49.31	40.70	40.09	40.11	41.11	50.08	50.87	50.38
TiO2	0.00	0.00	0.00	0.00	0.03	0.17	0.18	0.06	0.15	0.00	0.00	0.01
Al2O3	0.20	0.17	0.33	0.24	0.30	13.15	13.09	13.85	13.62	0.30	0.31	0.63
FeO	41.84	41.75	42.31	42.22	41.93	29.12	28.24	28.12	27.74	39.95	39.69	40.18
MnO	0.24	0.22	0.21	0.20	0.14	0.11	0.08	0.06	0.08	0.26	0.28	0.19
MgO	4.59	4.65	4.75	5.07	4.89	2.09	2.08	1.96	1.98	5.70	5.94	5.23
CaO	0.43	0.41	0.42	0.29	0.38	12.26	10.84	11.20	10.86	0.32	0.27	0.53
Na2O	0.05	0.10	0.05	0.03	0.10	1.43	1.55	1.60	1.69	0.10	0.11	0.13
K2O	0.00	0.00	0.00	0.00	0.00	0.42	0.36	0.48	0.43	0.00	0.00	0.00
Total	97.60	97.38	97.52	97.43	97.09	99.45	96.51	97.42	97.65	97.42	97.47	97.70
Cations based on 23 O												
Si	8.0589	8.0529	7.9741	7.9666	7.9765	6.3573	6.4151	6.3569	6.4636	8.0750	8.0710	8.0582
Ti	0.0000	0.0000	0.0000	0.0000	0.0040	0.0195	0.0217	0.0066	0.0179	0.0000	0.0000	0.0014
Al	0.0384	0.0329	0.0633	0.0460	0.0575	2.4213	2.4690	2.5865	2.5237	0.0570	0.0572	0.1181
Fe	5.6119	5.6143	5.7052	5.6958	5.6707	3.8032	3.7794	3.7261	3.6467	5.3094	5.2660	5.3298
Mn	0.0323	0.0300	0.0290	0.0273	0.0192	0.0143	0.0109	0.0083	0.0101	0.0347	0.0381	0.0250
Mg	1.0968	1.1148	1.1415	1.2195	1.1800	0.4875	0.4952	0.4620	0.4635	1.3505	1.4042	1.2377
Ca	0.0746	0.0700	0.0718	0.0493	0.0658	2.0579	1.8593	1.9015	1.8290	0.0541	0.0467	0.0896
Na	0.0157	0.0297	0.0167	0.0096	0.0324	0.4315	0.4813	0.4921	0.5165	0.0294	0.0323	0.0409
K	0.0000	0.0000	0.0000	0.0000	0.0000	0.0835	0.0729	0.0964	0.0860	0.0000	0.0000	0.0000
Sum	14.9286	14.9446	15.0016	15.0141	15.0061	15.6760	15.6048	15.6364	15.5570	14.9101	14.9155	14.9007
Fe/(Fe+Mg)	0.8365	0.8343	0.8333	0.8237	0.8278	0.8864	0.8842	0.8897	0.8872	0.7972	0.7895	0.8115

Sample	BH2030A	BH2030A	BH2030A	BH2047	BH2047	BH2047	BH2047	BH2047	BH2047	BH2047	BH2031C	BH2031C
Type	MIN	MIN	MIN	UM	UM	UM	UM	UM	UM	UM	MIN	MIN
Mineral	GRU	GRU	HBL	GRU	GRU	GRU	GRU	HBL	HBL	HBL	GRU	GRU
SiO2	50.37	50.64	40.38	49.80	50.19	50.83	49.16	41.01	41.79	40.41	50.93	49.43
TiO2	0.01	0.00	0.22	0.01	0.00	0.14	0.00	0.08	0.07	0.09	0.00	0.00
Al2O3	0.28	0.23	13.07	0.27	0.28	0.37	0.30	13.20	12.29	13.33	0.22	0.19
FeO	39.61	39.29	27.70	40.48	39.66	39.08	40.33	27.10	27.41	27.98	41.54	40.96
MnO	0.22	0.20	0.05	0.04	0.03	0.03	0.05	0.00	0.00	0.04	0.31	0.32
MgO	6.05	6.25	2.62	6.09	6.49	6.49	6.56	2.76	2.96	2.75	6.22	6.05
CaO	0.36	0.39	11.04	0.36	0.41	0.45	0.31	11.06	11.30	10.93	0.37	0.55
Na2O	0.12	0.04	1.56	0.05	0.06	0.00	0.06	1.30	1.18	1.33	0.02	0.06
K2O	0.00	0.00	0.42	0.00	0.00	0.00	0.00	0.40	0.38	0.33	0.00	0.00
Total	97.04	97.05	97.08	97.08	97.12	97.39	96.77	96.92	97.38	97.19	99.61	97.55
Cations based on 23 O												
Si	8.0395	8.0609	6.4080	7.9832	8.0027	8.0414	7.9179	6.4767	6.5731	6.3984	7.9718	7.9292
Ti	0.0017	0.0000	0.0266	0.0016	0.0000	0.0164	0.0000	0.0091	0.0087	0.0106	0.0000	0.0000
Al	0.0534	0.0433	2.4449	0.0501	0.0526	0.0685	0.0578	2.4577	2.2773	2.4866	0.0407	0.0351
Fe	5.2859	5.2292	3.6750	5.4256	5.2887	5.1691	5.4311	3.5796	3.6049	3.7052	5.4364	5.4946
Mn	0.0299	0.0274	0.0070	0.0050	0.0044	0.0045	0.0069	0.0000	0.0000	0.0048	0.0415	0.0434
Mg	1.4404	1.4823	0.6200	1.4549	1.5436	1.5313	0.5750	0.6496	0.6938	0.6496	1.4511	1.4469
Ca	0.0608	0.0665	1.8775	0.0616	0.0694	0.0758	0.0537	0.8717	1.9034	1.8534	0.0623	0.0937
Na	0.0387	0.0138	0.4811	0.0145	0.0173	0.0000	0.0195	0.3986	0.3584	0.4088	0.0063	0.0186
K	0.0000	0.0000	0.0851	0.0000	0.0000	0.0000	0.0000	0.0812	0.0766	0.0672	0.0000	0.0000
Sum	14.9503	14.9234	15.6252	14.9965	14.9787	14.9070	14.0619	14.5242	15.4962	15.5846	15.0101	15.0615
Fe/(Fe+Mg)	0.7859	0.7791	0.8556	0.7885	0.7741	0.7715	0.9043	0.8464	0.8386	0.8508	0.7893	0.7916

Sample	BH2031C	BH2031C	BH2031C	BH2031C	BH2031C	BH2031C	BH2031C	BH2031C	BH2031C	BH2031C	BH2031C	BH2031A
Type	MIN	MIN	MIN	MIN	MIN	MIN	MIN	MIN	MIN	MIN	MIN	MIN
Mineral	GRU	GRU	GRU	GRU	GRU	GRU	GRU	GRU	GRU	GRU	BT	GRU
SiO2	49.83	49.47	50.95	50.22	50.53	50.20	50.96	49.09	49.22	49.15	30.34	49.61
TiO2	0.00	0.00	0.00	0.00	0.00	0.00	0.00	0.01	0.00	0.00	0.67	0.00
Al2O3	0.18	0.29	0.18	0.26	0.21	0.23	0.21	0.32	0.30	0.20	14.76	0.19
FeO	41.34	40.27	40.94	40.89	39.97	41.32	39.84	41.75	41.52	40.09	35.36	42.13
MnO	0.34	0.33	0.35	0.25	0.28	0.29	0.25	0.25	0.25	0.27	0.02	0.17
MgO	6.20	6.96	6.52	6.65	7.81	6.49	7.40	6.02	6.16	7.55	4.73	4.62
CaO	0.37	0.38	0.39	0.39	0.44	0.37	0.40	0.27	0.41	0.38	0.02	0.64
Na2O	0.04	0.09	0.04	0.07	0.07	0.00	0.04	0.09	0.02	0.05	0.04	0.07
K2O	0.00	0.00	0.00	0.00	0.00	0.00	0.00	0.00	0.00	0.00	6.79	0.00
Total	98.29	97.79	99.37	98.74	99.30	98.91	99.09	97.81	97.87	97.69	92.75	97.44
Cations based on 23 O												
Si	7.9305	7.8856	7.9749	7.9262	7.8912	7.9249	7.9561	7.8818	7.8868	7.8433	5.4168	8.0030
Ti	0.0000	0.0000	0.0000	0.0000	0.0000	0.0000	0.0000	0.0018	0.0000	0.0000	0.0896	0.0000
Al	0.0340	0.0550	0.0340	0.0491	0.0382	0.0425	0.0395	0.0610	0.0559	0.0381	3.1061	0.0336
Fe	5.5013	5.3672	5.3485	5.3962	5.2205	5.4549	5.2009	5.6057	5.5630	5.3491	5.2781	5.6833
Mn	0.0454	0.0439	0.0462	0.0340	0.0364	0.0392	0.0334	0.0334	0.0342	0.0370	0.0037	0.0238
Mg	1.4707	1.6551	1.5222	1.5651	1.8180	1.5281	1.7215	1.4416	1.4710	1.7964	1.2599	1.1102
Ca	0.0635	0.0655	0.0656	0.0667	0.0732	0.0634	0.0661	0.0462	0.0698	0.0658	0.0048	0.1105
Na	0.0121	0.0276	0.0120	0.0222	0.0277	0.0000	0.0112	0.0267	0.0074	0.0140	0.0144	0.0208
K	0.0000	0.0000	0.0000	0.0000	0.0000	0.0000	0.0000	0.0000	0.0000	0.0000	1.5465	0.0000
Sum	15.0575	15.0999	15.0034	15.0595	15.1052	15.0530	15.0287	15.0982	15.0881	15.1437	16.7199	14.9852
Fe/(Fe+Mg)	0.7891	0.7643	0.7785	0.7752	0.7417	0.7812	0.7513	0.7954	0.7909	0.7486	0.8073	0.8366

Sample	BH2031A	BH2031A	BH2031A	BH2031A	BH2075A	BH2075A	BH2075A	BH2075A	BH2075A	BH2075A	BH2075A	BH2075A
Type	MIN	MIN	MIN	MIN	UM	UM	UM	UM	UM	UM	UM	UM
Mineral	GRU	GRU	GRU	HBL	GRU	GRU	GRU	GRU	GRU	GRU	GRU	HBL
SiO2	49.71	49.61	49.63	42.35	50.08	49.86	49.64	50.08	49.74	51.18	50.97	40.75
TiO2	0.00	0.03	0.01	0.27	0.03	0.00	0.04	0.00	0.00	0.01	0.02	0.14
Al2O3	0.18	0.18	0.24	9.26	0.25	0.24	0.14	0.18	0.23	0.30	0.28	12.90
FeO	41.33	41.62	41.51	30.75	42.36	41.91	42.30	40.82	42.65	41.61	40.64	20.66
MnO	0.22	0.16	0.19	0.05	0.10	0.01	0.02	0.04	0.07	0.05	0.08	0.08
MgO	4.59	4.95	4.75	2.28	5.06	4.93	5.44	6.39	5.45	5.60	5.76	2.22
CaO	0.52	0.39	0.45	10.50	0.43	0.34	0.31	0.22	0.34	0.21	0.25	10.79
Na2O	0.10	0.07	0.12	1.25	0.04	0.06	0.07	0.08	0.08	0.11	0.00	1.26
K2O	0.00	0.00	0.00	0.37	0.00	0.00	0.00	0.00	0.00	0.00	0.00	0.45
Total	96.65	97.02	96.89	97.09	98.35	97.35	97.97	97.80	98.55	99.11	98.00	97.45
Cations based on 23 O												
Si	8.0524	8.0128	8.0249	6.7947	7.9880	8.0203	7.9564	7.9722	7.9354	8.0369	8.0637	6.4598
Ti	0.0000	0.0037	0.0014	0.0328	0.0032	0.0000	0.0049	0.0000	0.0000	0.0018	0.0024	0.0168
Al	0.0348	0.0340	0.0462	1.7515	0.0471	0.0461	0.0267	0.0341	0.0425	0.0548	0.0519	2.4110
Fe	5.5984	5.6214	5.6123	4.1262	5.6498	5.6372	5.6696	5.4335	5.6891	5.4630	5.3771	3.8247
Mn	0.0300	0.0225	0.0254	0.0074	0.0129	0.0019	0.0030	0.0048	0.0095	0.0070	0.0112	0.0102
Mg	1.1091	1.1915	1.1438	0.5461	1.2038	1.1817	1.3004	1.5154	1.2956	1.3100	1.3586	0.5241
Ca	0.0895	0.0680	0.0776	1.8052	0.0738	0.0593	0.0529	0.0370	0.0579	0.0430	0.0420	1.8325
Na	0.0303	0.0233	0.0362	0.3890	0.0113	0.0182	0.0211	0.0259	0.0248	0.0332	0.0000	0.3876
K	0.0000	0.0000	0.0000	0.0749	0.0000	0.0000	0.0000	0.0000	0.0000	0.0000	0.0000	0.0910
Sum	14.9445	14.9772	14.9678	15.5278	14.9899	14.9647	15.0350	15.0229	15.0548	14.9497	14.9069	15.5577
Fe/(Fe+Mg)	0.8346	0.8251	0.8307	0.8831	0.8244	0.8267	0.8134	0.7819	0.8145	0.8066	0.7983	0.8795

Sample	BH2075A	BH2075B	BH2075B	BH2075B	BH2075B	BH2075B	BH2075B	BH2075B	BH2075B	BH2075B	BH2075B	BH1073B
Type	UM	UM	UM	UM	UM	UM	UM	UM	UM	UM	UM	UM
Mineral	HBL	GRU	GRU	GRU	GRU	GRU	GRU	HBL	HBL	HBL	HBL	GRU
SiO2	41.08	50.80	50.71	50.80	50.49	49.34	50.31	40.58	40.71	40.48	38.49	50.83
TiO2	0.14	0.00	0.00	0.00	0.00	0.02	0.02	0.05	0.05	0.08	0.02	0.02
Al2O3	12.86	0.18	0.24	0.25	0.22	0.23	0.36	13.79	14.38	14.39	14.25	0.42
FeO	28.33	42.27	42.39	41.86	42.38	43.48	42.85	29.00	28.40	28.39	30.48	40.54
MnO	0.00	0.11	0.05	0.07	0.02	0.07	0.03	0.07	0.00	0.00	0.00	0.15
MgO	2.11	5.25	4.63	5.04	4.73	3.92	4.60	1.50	1.53	1.64	2.04	6.17
CaO	10.90	0.24	0.33	0.30	0.31	0.31	0.27	10.79	11.11	11.15	9.02	0.34
Na2O	1.23	0.09	0.07	0.06	0.07	0.00	0.13	1.10	1.09	1.19	1.11	0.09
K2O	0.48	0.00	0.00	0.00	0.00	0.00	0.00	0.48	0.49	0.50	0.53	0.00
Total	97.13	98.94	98.42	98.37	98.22	97.37	98.58	97.37	97.75	97.81	95.94	98.57
Cations based on 23 O												
Si	6.5103	8.0287	8.0627	8.0576	8.0485	8.0082	8.0123	6.4323	6.4037	6.3726	6.2423	8.0004
Ti	0.0172	0.0000	0.0000	0.0000	0.0000	0.0240	0.0023	0.0084	0.0058	0.0090	0.0026	0.0028
Al	2.4012	0.0337	0.0443	0.0471	0.0416	0.0440	0.0673	2.5751	2.6656	2.6689	2.7236	0.0772
Fe	3.7539	5.5858	5.6362	5.5526	5.6498	5.9012	5.7064	3.8435	3.7362	3.7362	4.1329	5.3356
Mn	0.0000	0.0147	0.0072	0.0090	0.0023	0.0096	0.0040	0.0091	0.0000	0.0000	0.0000	0.0203
Mg	0.4991	1.2365	1.0975	1.1916	1.1249	0.9478	1.0925	0.3552	0.3580	0.3849	0.4933	1.4487
Ca	1.8510	0.0399	0.0558	0.0516	0.0526	0.0532	0.0465	1.8326	1.8725	1.8795	1.5673	0.0581
Na	0.3788	0.0282	0.0210	0.0171	0.0202	0.0000	0.0412	0.3388	0.3329	0.3635	0.3503	0.0280
K	0.0877	0.0000	0.0000	0.0000	0.0000	0.0000	0.0000	0.0980	0.0974	0.1003	0.1101	0.0000
Sum	15.4992	14.9675	14.9247	14.9266	14.9399	14.9880	14.9725	15.4910	15.4721	15.5149	15.6224	14.9711
Fe/(Fe+Mg)	0.8826	0.8188	0.8370	0.8233	0.8340	0.8616	0.8393	0.9154	0.9126	0.9066	0.8934	0.7865

Sample	BH1073B	BH1073B	BH1073B	BH1073B	BH1073B	BH1073B	BH1073B	BH1073B	BH1037	BH1037	BH1037	BH1037
Type	UM	UM	UM	UM	UM	UM	UM	UM	UM	UM	UM	UM
Mineral	GRU	GRU	GRU	GRU	GRU	GRU	GRU	GRU	GRU	GRU	GRU	GRU
SiO2	51.36	51.48	50.20	50.62	50.51	51.10	50.89	50.64	50.09	50.07	50.66	50.13
TiO2	0.03	0.00	0.00	0.00	0.00	0.00	0.02	0.03	0.00	0.00	0.00	0.00
Al2O3	0.07	0.07	0.12	0.16	0.24	0.21	0.30	0.37	0.26	0.20	0.30	0.39
FeO	40.57	39.64	41.36	40.62	40.42	40.67	40.66	40.39	41.09	41.33	40.83	41.13
MnO	0.19	0.13	0.14	0.13	0.13	0.16	0.10	0.11	0.13	0.10	0.13	0.11
MgO	6.43	6.44	6.15	5.91	5.95	6.13	6.32	6.13	5.36	5.45	5.86	5.45
CaO	0.20	0.16	0.19	0.22	0.16	0.23	0.25	0.28	0.22	0.25	0.23	0.30
Na2O	0.05	0.00	0.17	0.10	0.04	0.10	0.07	0.10	0.00	0.09	0.00	0.02
K2O	0.00	0.00	0.02	0.00	0.00	0.00	0.00	0.00	0.00	0.00	0.00	0.00
Total	98.89	97.92	98.34	97.75	97.44	98.61	98.60	98.05	97.15	97.48	98.00	97.53
Cations based on 23 O												
Si	8.0461	8.1028	7.9703	8.0442	8.0434	8.0390	8.0072	8.0113	8.0374	8.0184	8.0311	8.0124
Ti	0.0036	0.0000	0.0000	0.0000	0.0000	0.0000	0.0023	0.0031	0.0000	0.0000	0.0000	0.0000
Al	0.0130	0.0134	0.0228	0.0292	0.0448	0.0382	0.0556	0.0689	0.4880	0.0375	0.0562	0.0730
Fe	5.3140	5.2172	5.4911	5.3972	5.3826	5.3499	5.3488	5.3435	5.5130	5.5350	5.4124	5.4961
Mn	0.0247	0.0170	0.0183	0.0173	0.0176	0.0216	0.0139	0.0148	0.0171	0.0134	0.0169	0.0150
Mg	1.5016	1.5116	1.4546	1.3993	1.4118	1.4371	1.4818	1.4454	1.2825	1.3012	1.3846	1.2992
Ca	0.0328	0.0276	0.0315	0.0372	0.0275	0.0395	0.0421	0.0480	0.0386	0.0421	0.0386	0.0514
Na	0.0146	0.0000	0.0530	0.0320	0.0112	0.0316	0.0205	0.0302	0.0000	0.0287	0.0000	0.0062
K	0.0000	0.0000	0.0043	0.0000	0.0000	0.0000	0.0000	0.0000	0.0000	0.0000	0.0000	0.0000
Sum	14.9504	14.8896	15.0459	14.9564	14.9389	14.9569	14.9722	14.9652	15.3766	14.9763	14.9398	14.9533
Fe/(Fe+Mg)	0.7797	0.7754	0.7906	0.7941	0.7922	0.7883	0.7831	0.7871	0.8113	0.8097	0.7963	0.8088

Sample	BH1037	BH1037	BH1037	BH1037	BH1004B-1	BH1004B-1	BH1004B-1	BH1004B-1	BH1004B-1	BH1004B-1	BH1004B-1	BH1004B-1
Type	UM	UM	UM	UM	UM	UM	UM	UM	UM	UM	UM	UM
Mineral	GRU	GRU	GRU	GRU	GRU	GRU	GRU	GRU	GRU	GRU	GRU	GRU
SiO2	49.77	49.74	50.17	50.73	49.30	49.62	49.94	50.13	49.59	49.89	50.19	49.62
TiO2	0.00	0.02	0.00	0.02	0.00	0.00	0.00	0.00	0.03	0.00	0.02	0.00
Al2O3	0.37	0.47	0.46	0.36	0.39	0.40	0.31	0.28	0.44	0.41	0.45	0.46
FeO	40.42	40.25	39.76	40.47	41.85	41.45	42.45	41.04	41.65	41.46	39.76	40.56
MnO	0.13	0.11	0.13	0.09	0.08	0.10	0.10	0.13	0.04	0.05	0.08	0.08
MgO	6.19	6.42	6.74	6.16	4.60	5.34	4.91	5.35	5.33	5.17	6.54	6.59
CaO	0.21	0.23	0.22	0.27	0.29	0.36	0.30	0.27	0.37	0.45	0.25	0.22
Na2O	0.06	0.16	0.05	0.04	0.09	0.10	0.09	0.10	0.11	0.06	0.16	0.11
K2O	0.00	0.00	0.00	0.00	0.00	0.00	0.00	0.00	0.00	0.00	0.00	0.00
Total	97.14	97.40	97.53	98.14	96.57	97.38	98.09	97.29	97.56	97.49	97.43	97.63
Cations based on 23 O												
Si	7.9717	7.9413	7.9667	8.0162	8.0083	7.9725	7.9915	8.0321	7.9583	7.9979	7.9787	7.9145
Ti	0.0000	0.0022	0.0000	0.0018	0.0000	0.0000	0.0000	0.0000	0.0037	0.0000	0.0019	0.0000
Al	0.0692	0.0884	0.0861	0.0661	0.0745	0.0752	0.0577	0.0530	0.0834	0.0777	0.0837	0.0856
Fe	5.4130	5.3729	5.2795	5.3477	5.6846	5.5886	5.6799	5.4990	5.5885	5.5576	5.2848	5.4098
Mn	0.0176	0.0147	0.0172	0.0125	0.0078	0.0137	0.0134	0.0173	0.0056	0.0066	0.0103	0.0108
Mg	1.4769	1.5290	1.5945	1.4513	1.1133	1.2800	1.1706	1.2779	1.2748	1.2353	1.5500	1.5660
Ca	0.0357	0.0386	0.0373	0.0454	0.0502	0.0626	0.0520	0.0460	0.0636	0.0775	0.0420	0.0377
Na	0.0177	0.0486	0.0161	0.0137	0.0293	0.0327	0.0272	0.0301	0.0350	0.0194	0.0501	0.0345
K	0.0000	0.0000	0.0000	0.0000	0.0000	0.0000	0.0000	0.0000	0.0000	0.0000	0.0000	0.0000
Sum	15.0018	15.0357	14.9974	14.9547	14.9680	15.0053	14.9923	14.9554	15.0129	14.9720	15.0015	15.0589
Fe/(Fe+Mg)	0.7856	0.7785	0.7680	0.7865	0.8362	0.8131	0.8291	0.8114	0.8143	0.8181	0.7732	0.7755

Sample	BH1004B-1	BH1073A	BH1073A	BH1073A	BH1073A	BH1073A	BH1073A	BH1073A	BH1073A	BH1073A	BH1073A
Type	UM	UM	UM	UM	UM	UM	UM	UM	UM	UM	UM
Mineral	GRU	GRU	GRU	GRU	GRU	GRU	GRU	GRU	GRU	GRU	GRU
SiO2	49.55	49.99	50.36	50.50	50.20	50.39	51.11	50.39	50.42	50.05	50.17
TiO2	0.00	0.00	0.03	0.01	0.00	0.00	0.03	0.00	0.00	0.00	0.02
Al2O3	0.36	0.17	0.23	0.24	0.24	0.22	0.09	0.11	0.20	0.11	0.11
FeO	41.70	41.73	42.43	42.19	41.87	42.16	41.36	41.67	41.43	41.06	41.01
MnO	0.09	0.14	0.15	0.06	0.16	0.10	0.12	0.06	0.08	0.15	0.13
MgO	5.46	4.86	4.82	4.65	4.85	4.95	5.40	5.50	5.39	5.40	5.61
CaO	0.26	0.20	0.20	0.23	0.24	0.22	0.14	0.17	0.19	0.20	0.20
Na2O	0.12	0.07	0.03	0.03	0.02	0.00	0.10	0.10	0.06	0.02	0.00
K2O	0.00	0.00	0.00	0.00	0.00	0.00	0.00	0.00	0.00	0.00	0.00
Total	97.54	97.17	98.25	97.91	97.59	98.03	98.35	98.00	97.78	96.99	97.25
Cations based on 23 O											
Si	7.9571	8.0490	8.0313	8.0670	8.0460	8.0421	8.0837	8.0284	8.0410	8.0480	8.0391
Ti	0.0000	0.0000	0.0031	0.0016	0.0000	0.0000	0.0033	0.0000	0.0000	0.0000	0.0021
Al	0.0689	0.0324	0.0433	0.0443	0.0457	0.0405	0.0176	0.0211	0.0379	0.0200	0.0205
Fe	5.6000	5.6192	5.6592	5.6354	5.6112	5.6267	5.4697	5.5524	5.5250	5.5202	5.4950
Mn	0.0117	0.0196	0.0205	0.0087	0.0222	0.0138	0.0161	0.0084	0.0112	0.0207	0.0180
Mg	1.3071	1.1669	1.1454	1.1076	1.1599	1.1768	1.2737	1.3054	1.2813	1.2941	1.3390
Ca	0.0443	0.0352	0.0350	0.0391	0.0420	0.0369	0.0243	0.0297	0.0330	0.0345	0.0339
Na	0.0366	0.0228	0.0102	0.0094	0.0083	0.0000	0.0299	0.0294	0.0194	0.0070	0.0000
K	0.0000	0.0000	0.0000	0.0000	0.0000	0.0000	0.0000	0.0000	0.0000	0.0000	0.0000
Sum	15.0257	14.9451	14.9480	14.9131	14.9333	14.9368	14.9183	14.9748	14.9488	14.9445	14.9476
Fe/(Fe+Mg)	0.8108	0.8280	0.8317	0.8357	0.8287	0.8270	0.8111	0.8096	0.8117	0.8101	0.8041